# Investigating Distinct Topological Surface States in Hexagonal ABC-type 3D Dirac Semimetal

Jimin Kim[a,b] , Seongyong Lee[a,b], Choongjae Won[b] and Jae-Hoon Park[a,b]

[a]*Department of Physics, POSTECH, Pohang, 37673, South Korea*
[b]*Max Planck POSTECH/Korea Research Initiative, Center for Complex Phases of Materials, Pohang, 37673, South Korea*

**Keywords:** Dirac Semimetal, Weyl semimetal, ARPES, spin

Topological semimetals are typically classified as either Dirac or Weyl, based on symmetries that have long appeared mutually exclusive [1-3]. Dirac semimetals require both time-reversal and inversion symmetry, whereas Weyl semimetals necessitate that one of these symmetries be broken. Realizing both phases in a single material is therefore challenging. One potential solution is to utilize different crystal facets that host distinct topological states due to their unique bulk-boundary correspondence [4].

Here, we report on spin- and angle-resolved photoemission spectroscopy (spin-ARPES) measurements of the polar hexagonal ABC-type crystal SrAuBi. This material undergoes a structural phase transition below approximately 214 K that breaks inversion symmetry while preserving the rotational symmetry required to protect Dirac points [5]. This low-temperature phase is theoretically predicted to allow for the coexistence of both Dirac and Weyl features on different crystal surfaces.

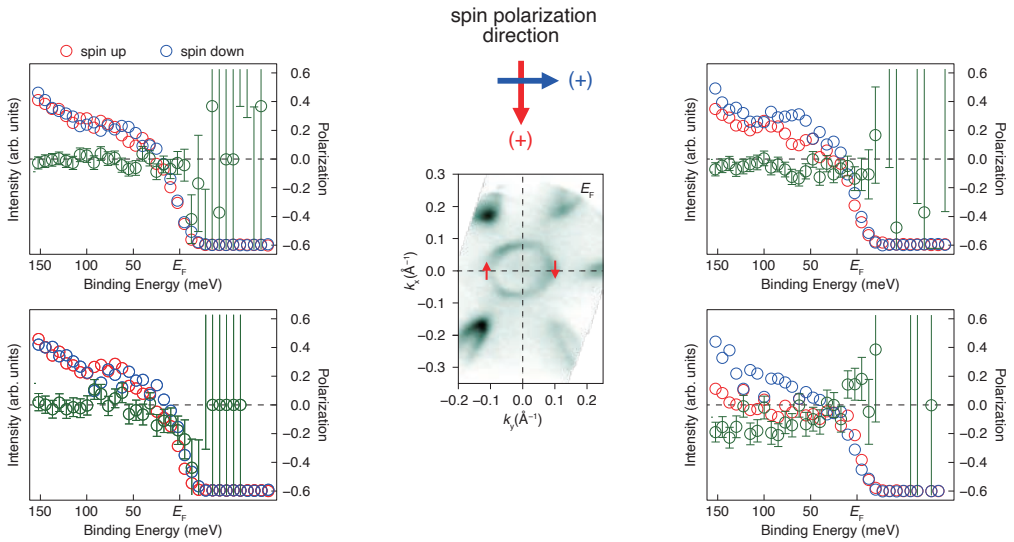


**FIGURE 1.** The obtained Fermi surface of SrAuBi and corresponding spin polarization measurement results. The direction of spin polarization is illustrated as overlaid red arrows on the Fermi surface.

Our measurements of the (001) top surface of SrAuBi reveal distinct surface states, as shown in Fig. 1. The data show a hexagonal electron pocket at the Brillouin zone center and six leaf-like features extending toward the zone boundaries. We attribute these features to Weyl fermion-induced surface states, which originate from the buckled honeycomb AuBi layer where inversion symmetry is broken.

To confirm their topological nature, we measured the spin polarization of these surface states. As

presented in Fig. 1, the spin polarization is oppositely oriented on either side of the zone center, demonstrating a chiral spin texture. This observation corroborates the topological origin of the surface states and confirms the existence of a Weyl semimetal phase on the top surface of SrAuBi. These results motivate future work, including an investigation of the side surface of the SrAuBi crystal to search for the predicted Dirac semimetal phase, alongside theoretical calculations to fully validate our findings.

## REFERENCES


1. N. P. Armitage *et al.*, *Rev. Mod. Phys.* **90**, 015001 (2018).
2. Q. D. Gibson *et al.*, *Phys. Rev. B* **91**, 205128 (2015).
3. H. Gao *et al.*, *Phys. Rev. Lett.* **121**, 106404 (2018).
4. N. Avraham *et al.*, *Nat. Mater.* **19**, 610 (2020).
5. H. Takahashi *et al.*, *npj Quantum Mater.* **8**, 77 (2023).

# A laser spin ARPES study of antiferromagnetic thin films

Yuita Fujisawa[a], Takuma Iwata[b, c], Kenta Kuroda[b, c]

[a] *Research Institute for Synchrotron Radiation Science, Hiroshima university, 2-313, Kagamiyama, Higashi-Hiroshima, Hiroshima, 739-0024, Japan.*
[b] *Graduate School of Advanced Science and Engineering, Hiroshima University, 1-3-1 Kagamiyama, Higashi-Hiroshima, Hiroshima 739-8526, Japan.*
[c] *International Institute for Sustainability with Knotted Meta Matter (WPI-SKCM$^2$) Hiroshima University, 2-313 Kagamiyama, Higashi-Hiroshima, Hiroshima 739-0046, Japan*

**Keywords:** antiferromagnet, spin-ARPES, altermagnet, molecular beam epitaxy

In recent years, a new class of magnetic materials known as altermagnets has attracted significant attention. Like antiferromagnets, these materials exhibit no net macroscopic magnetization; however, they possess spin-polarized band structures similar to those found in ferromagnets. Owing to this unique spin-polarized electronic state, a variety of intriguing physical phenomena are expected and, in some cases, have already been experimentally demonstrated [1,2]. To verify whether such spin-polarized electronic states are indeed realized, researchers worldwide have attempted to directly observe them using spin- and angle-resolved photoemission spectroscopy (SARPES). Nevertheless, a clear observation has not yet been achieved, primarily due to two challenges: (i) the difficulty of cleaving their inherently three-dimensional crystals to obtain clean surfaces, and (ii) the averaging out of spin polarization signals caused by the presence of microscopic magnetic domains.

The goal of this project is to directly observe the spin-polarized electronic states of altermagnets, which have so far proven technically challenging to detect. We focus on MnTe, one of the most extensively studied altermagnet candidates. A key feature of our approach is the use of MnTe thin films grown by molecular beam epitaxy (MBE) as measurement samples. This thin-film approach eliminates concerns about surface roughness or inhomogeneity associated with crystal cleaving. More importantly, by employing a micro-focused laser as the light source, we aim to selectively probe individual magnetic domains, thereby enabling the clear detection of spin-polarized electronic states [3].

Figure 1a shows the Fermi surface obtained by integrating the photoemission intensity over an energy window of $E$-$E_F$=0±20 meV. A circular constant-energy contour is clearly observed. The band dispersion along the $k_x$ ($\bar{\Gamma}$–$\bar{M}$) direction is shown in Fig. 1b, where a hole band crossing the Fermi level is evident. We next performed spin energy distribution curve (spin-EDC) measurements at the two opposite momenta $\pm k_F$ indicated in Fig. 1b. In both cases, no clear spin polarization was detected, as shown in Fig. 1c and 1d. We attribute this absence to the magnetic/structural domain size being much smaller than the laser spot size (~10 μm) [4]. To achieve unambiguous visualization of spin polarization, it will be necessary to control the magnetic domains— for example, by applying a magnetic field prior to measurement and/or by employing the magnetic proximity effect from a ferromagnetic substrate into MnTe thin films.

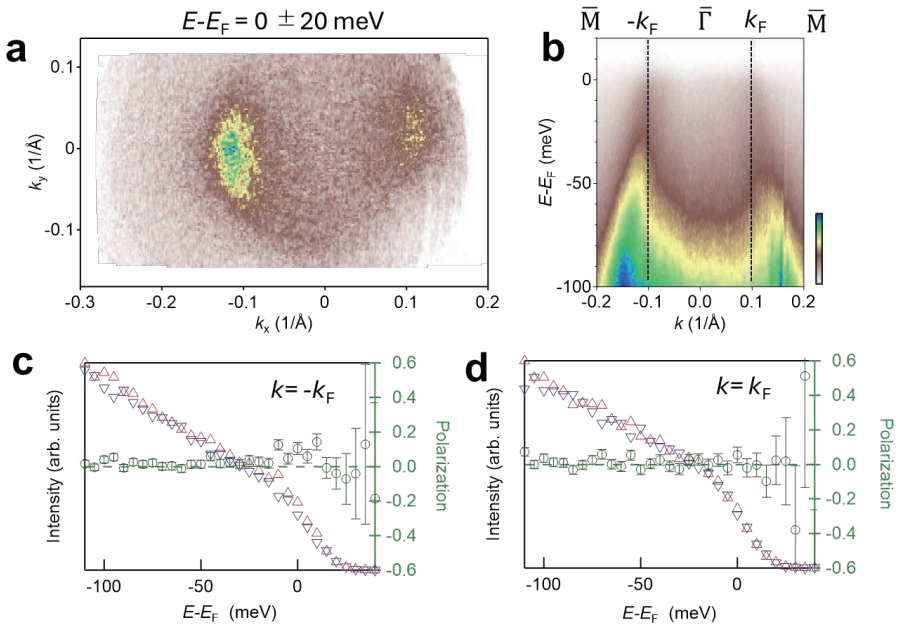


**FIGURE 1.** (a) Fermi surface obtained by laser-spin ARPES ($h\nu$=6.3 eV). (b) Energy dispersion along $k_x$ direction parallel to $\bar{\Gamma}\bar{M}$ at $k_y = 0$ in (a). (c,d) Spin energy distribution curves (red, blue), and spin polarization (green) taken at $k = -k_F$ and $k_F$, respectively.

## REFERENCES


1. L. Smejkal et al., Phys. Rev. X **12**, 040501 (2022).
2. L. Smejkal et al., Nature Reviews Materials **7**, 482-496 (2022).
3. T. Iwata et al., Sci. Rep. **14**, 127 (2024).
4. O.J. Amin et al., Nature **636**, 348 (2024).

# Micro-Spin-ARPES Observation of Topological Surface States on Non-Cleavage Surfaces of Topological Insulators $Bi_2Te_3$

R. Yamamoto[a], S. Yokoyama[a,c], K. Kuroda[a,c,d] and T. Okuda [b,c,d]

[a]*Graduate School of Advanced Science and Engineering Hiroshima University, 1-3-1 Kagamiyama Higashi-Hiroshima 739-8526, Japan*
[b]*Research Institute for Synchrotron Radiation Science (HiSOR), Hiroshima University, 2-313 Kagamiyama, Higashi-Hiroshima 739-0046, Japan*
[c]*International Institute for Sustainability with Knotted Chiral Meta Matter (WPI-SCKM$^2$), Hiroshima University, 2-313 Kagamiyama, Higashi-Hiroshima 739-0046, Japan*
[d]*Research Institute for Semiconductor Engineering (RISE), Hiroshima University, 1-4-2 Kagamiyama, Higashi-Hiroshima 739-8527, Japan*

**Keywords:** Micro-spin-ARPES, Strong topological insulators, Topological surface states, Non-cleavage surface, Anisotropic band structure

Nearly two decades have passed since the discovery of topological insulators, and their surface electronic states have been observed in many topological insulators by angle-resolved photoemission spectroscopy (ARPES) and spin-resolved ARPES. The prototypical three-dimensional topological insulators $Bi_2Te_3$ is classified as strong topological insulators, in which topological surface states (TSS) are theoretically expected to exist on all surfaces[1]. Indeed, many observations of clear TSS have been reported for this materials; however, all reports have been limited to the cleavage surfaces. To date, there has been no experimental verification of TSS on non-cleavage surfaces. Because these compounds are layered materials, its non-cleavage surfaces correspond to the edges of individual quintuple layers, where the electronic states are expected to be confined in one dimension. Such confinement effects are anticipated to modulate the electronic structure[2][3], leading to anisotropic TSS. Furthermore, in anisotropic TSS, enhanced suppression of backscattering is expected, which in turn could result in an extended spin relaxation length. This feature would be beneficial for realizing long-distance transport and spintronic applications.

In this study, we attempted to fracture three-dimensional topological insulator, $Bi_2Te_3$ along surfaces other than the normal cleavage plane and investigated the electronic structure of these fractured surfaces by ARPES and spin-resolved ARPES. The goal was to examine the anisotropy of the surface band structure and the presence of spin polarization. As shown in Fig. 1, $Bi_2Te_3$ single crystal whose crystallographic orientation was determined, was fixed to a sample holder with silver paste. A post with a slit was attached to the exposed side of the crystal, and the post was knocked off to fracture along the non-cleavage surface. Since $Bi_2Te_3$ is layered material, the fractured surfaces may become rough, resulting in extremely small regions suitable for measurement. To overcome this, we used a Ti:sapphire laser beam focused down to 5–10 μm in diameter[3], enabling us to probe the band structure and spin polarization of the surface states in a small area.

For a sample mounted with the $\overline{\Gamma}$-$\overline{K}$ direction aligned horizontally, a Fermi surface elongated along the direction of the stacked layers (i.e., the direction of electronic confinement) is observed. We further examined the light-polarization dependence by using both *s*- and *p*-polarized light. With *s*-polarization, the Dirac cone is clearly observed on both sides of the wave vector (Fig. 2(a)), whereas with *p*-polarization the spectral intensity is significantly suppressed on one side (Fig. 2(b)). This light polarization dependence is consistent with that reported for TSS on the normal cleavage surface of $Bi_2Te_3$. We also tried to investigate spin polarization; however, the measurements were unsuccessful, most likely due to degradation of the crystal surface, or previously measured position on the surface was lost.

In contrast, for samples mounted with the $\overline{\Gamma}$-$\overline{M}$ direction aligned horizontally, we were unable to find regions to observe clear surface band structure, and consequently neither band structure nor spin-resolved measurements could be obtained.

In conclusion, we can observe the anisotropic topological surface states on non-cleavage surface of $Bi_2Te_3$. These results are expected to contribute the spintronics technology. In the future, we aim to measure the spun texture of the surface band and obtain a clearer understanding of the electronic structure of non-cleavage surfaces. We are also interested in further investigating to other crystal orientations and non-cleavage surfaces.

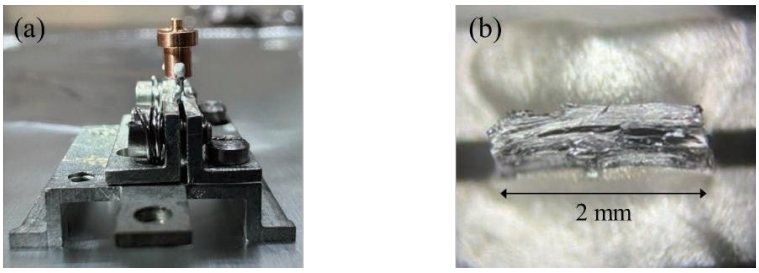


Figure 1：(a) Side view of sample. (b) Fractured surface of $Bi_2Te_3$ crystal.

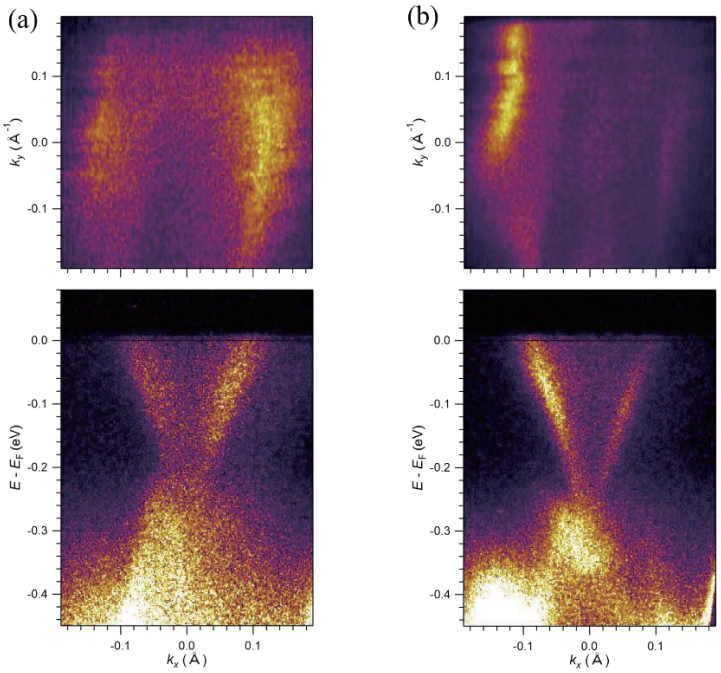


Fugure2：Fermi surface and surface band structure of $Bi_2Te_3$ non-cleavage surface measured by (a)*s*-polarization and (b)*p*-polarization.

## REFERENCES


1. W. Zhang *et al.,* New Journal of Physics **12**, 065013(2010)
2. N. Nagamura *et al.*, Phys. Rev. Lett. **96**, 256801 (2006).
3. J. Villanova *et al.*, Phys. Rev. B. **93**, 085122 (2016).
4. T. Iwata *et al.,* Sci. Rep. **14**, 127(2024)

# Activity and Characteristics of Ni-Based Hybrid Catalysts with Promoters for Ammonia Methanation

Reiji Sunamoto[a], Hiroki Miyaoka[a], Takayuki Ichikawa[a] and Hitoshi Saima[a]

[a]*Hiroshima University, Higashi-Hiroshima, Japan*

**Keywords:** carbon dioxide, ammonia, methane

**Background:**

As one of the carbon recycle techniques, we propose ammonia methanation, which directly synthesizes methane from carbon dioxide and ammonia. Ammonia methanation (1) is a combination of the Sabatier reaction (methane synthesis) (2) and ammonia decomposition (3).

$$CO_2 + 8/3\,NH_3 \rightarrow CH_4 + 4/3\,N_2 + 2H_2O \quad \Delta H = -42.5\ \text{kJ} \tag{1}$$

$$CO_2 + 4H_2 \rightarrow CH_4 + 2H_2O \quad \Delta H = -165.0\ \text{kJ} \tag{2}$$

$$8/3\,NH_3 \rightarrow 4/3\,N_2 + 4H_2 \quad \Delta H = -122.5\ \text{kJ} \tag{3}$$

Since the heat generation from ammonia methanation is about 1/4 compared with that of the Sabatier reaction (2), conventional adiabatic reactors can be used. On the other hand, the issue of ammonia methanation is that suitable catalysts to accelerate both reactions should be designed effectively. In a previous study, ammonia methanation was conducted using a hybrid catalyst consisting of $Ni/Al_2O_3$ for ammonia decomposition and $Ni/CeO_2$ for methane synthesis, achieving about 60% of methane yield at 500°C and 0.4 MPa. The ammonia decomposition rate in this condition was about 57%.[1] In this study, effective ammonia decomposition catalysts with promoters are prepared to enhance the catalysis at low-temperature regions, and their catalytic activity is investigated.

**Experimental Methods:**

$Ni/Al_2O_3$ (Ni: 10 wt%) was used as a catalyst for ammonia decomposition. Alkaline metals, which are K, Li, Na, K, Rb, and Cs, were added to the catalyst as promoters, where the number of promoters was 2 wt% to the Ni catalyst. The hybrid catalyst was prepared by mixing Ni-Ba/ $Al_2O_3$ and $Ni/CeO_2$(Ni: 20wt%) as a catalyst for ammonia methanation. The catalysts are characterized by X-ray absorption spectroscopy. (Quantum leap)

**Results and discussion:**

The results of ammonia decomposition at 500 °C by using the prepared catalysts with alkaline metals are shown as follows,

$$Ni/Al_2O_3\ (75\%) > K\ (71\%) > Na\ (67\%) > Cs\ (64\%) \approx Rb\ (63\%) > Li\ (51\%)$$

$Ni/Al_2O_3$ without a promoter showed the highest ammonia decomposition rate. Among the alkaline metal species, K showed the highest ammonia decomposition rate. A plot of the relationship between ammonia decomposition rate and electronegativity for catalysts with alkaline metal species showed a volcanic-type trend (Fig. 1). From the results, it was expected that the peak is in the region of 0.82~0.93, and the corresponding element is only Ba. Therefore, the catalyst with Ba was prepared, and its catalysis for the ammonia decomposition reaction was evaluated. As shown in Figure 1, the Ba-added catalysts showed the highest catalytic activity with a 77% decomposition rate. Fig.2 shows the XANES spectra. The spectrum

of Ni-Ba was slightly shifted to the oxidation side and different from the spectra of other catalysts. This chemical state might contribute to the highest catalytic activity of Ni-Ba.

The results of ammonia methanation experiments are shown in Fig. 3. The highest methane yield, 73%, was obtained by using the Ni catalyst at 550 °C and 0.5 MPa.

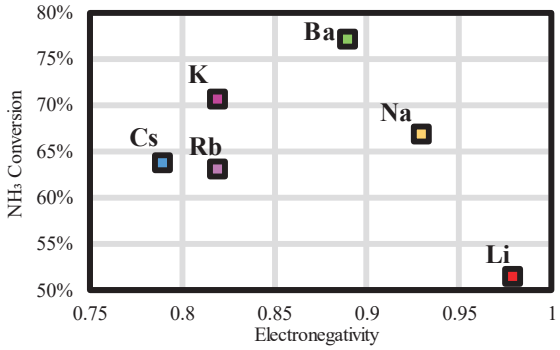


**FIGURE 1.** Relationship between ammonia decomposition rate and electronegativity

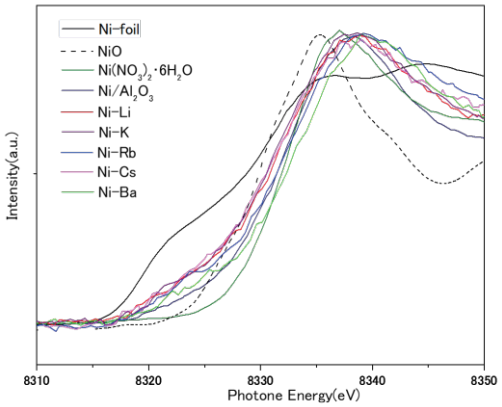


**FIGURE 2.** XANES spectra of the Ni-K edge.

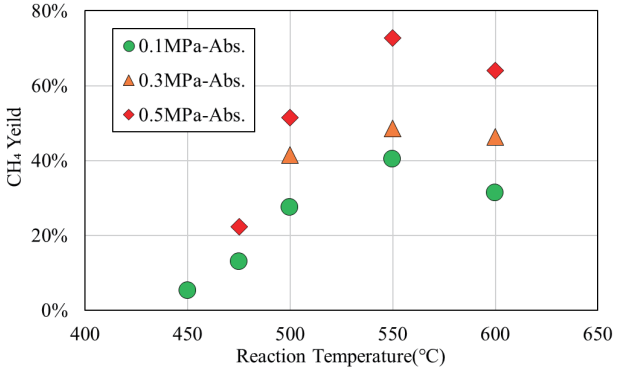


**FIGURE 3.** Methane yield of ammonia methanation with hybrid catalysts of Ni-Ba/$Al_2O_3$ and Ni/$CeO_2$

## REFERENCES

1. Hitoshi Saima, Reiji Sunamoto, Hiroki Miyaoka, and Takayuki Ichikawa, *Ammonia Methanation of Carbon Dioxide with a Hybrid Catalyst,* JOURNAL OF CHEMICAL ENGINEERING OF JAPAN, 2023, Volume 56.

# Structural Dynamics of β-Lactoglobulin in the Interaction Processes with Sodium Dodecyl Sulfate Micelles Observed by Time-Resolved Vacuum-Ultraviolet Circular Dichroism

Satoshi Hashimoto[a] and Koichi Matsuo[a,b,c]

*[a]Graduate School of Advanced Science and Engineering, Hiroshima University, 1-3-1 Kagamiyama, Higashi-Hiroshima 739-8526, Japan*
*[b]Research Institute for Synchrotron Radiation Science, Hiroshima University, 2-313 Kagamiyama, Higashi-Hiroshima 739-0046, Japan*
*[c]International Institute for Sustainability with Knotted Chiral Meta Matter (WPI-SKCM$^2$), Hiroshima University, 2-313 Kagamiyama, Higashi-Hiroshima 739-0046, Japan*

**Keywords:** Circular dichroism, β-Lactoglobulin, Membrane interaction, Secondary structures, Time-resolved measurement

Structural transition of proteins induced by the membrane interaction alter their biological function. Hence, the structural dynamics in the membrane-interaction processes is key information to elucidating the mechanisms of expressed function. While vacuum-ultraviolet circular dichroism (VUVCD) spectroscopy has been widely applied to the studies of membrane-bound structures of proteins[1,2], the previous investigations were limited to the static conditions (before and after membrane interaction). To address this, we developed a time-resolved VUVCD (TR-VUVCD) method, enabling real-time observation of structural dynamics[3]. This study analyzed the interaction processes between β-lactoglobulin (bLG) and sodium dodecyl sulfate (SDS) micelles using TR-VUVCD and molecular dynamics (MD) simulations. First, we obtained a TRCD dataset in the 178–260 nm wavelength range within one second, which reflected the structural transitions of bLG due to the SDS interaction. Our analysis identified a single intermediate state, revealing a step-by-step transition of the native (N-) state → intermediate (I-) state → micelle-bound (M-) state. Secondary structure analysis showed that the I-state formed six helices, which were extended and stabilized in the M-state. Second, we conducted the MD simulations to confirm the binding potential of these helices to the micelle surface. Our analysis on the physicochemical properties (charge, hydrophobicity) of each helix and MD-derived parameters such as peptide-micelle distance, hydrogen bonding, and micelle penetration, characterized the key driving forces on the interactions, in which electrostatic interactions contributed at the initial stage (I-state) while hydrophobic interactions played a significant role in stabilizing the final structure (M-state). These results demonstrate that TR-VUVCD combined with MD simulations is a powerful method for characterizing protein dynamics in the processes of membrane interaction, contributing to a deeper understanding of the mechanism of function expression at molecular level.

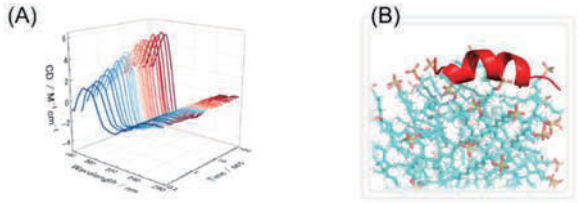


**FIGURE.** (A) TR-VUVCD data sets in the interaction process between bLG and SDS micelle. (B) The snapshot of MD simulation using Amber program.

## REFERENCES

1. K. Matsuo, K. Kumashiro, K. Gekko, *Chirality* **32**, 594-604 (2020)
2. R. Imaura, Y. Kawata, K. Matsuo, *Langmuir* **40**, 20537–20549 (2024)
3. S. Hashimoto and K. Matsuo, *Anal. Chem.* **96**, 10524-10533 (2024)

# Mechanistic Insights Into Oxidative Response of Heat Shock Factor 1 Condensates

Soichiro Kawagoe [a], Munehiro Kumashiro[a], Koichi Matsuo[b], and Tomohide Saio[a]

[a]*Institute of Advanced Medical Sciences, Tokushima University*
[b]*Research Institute for Synchrotron Radiation Science, Hiroshima University*

**Keywords:** heat shock factor 1, biological phase transition, stress response, circular dichroism.

Heat shock factor 1 (Hsf1), a hub protein in the stress response and cell fate decisions, senses the strength, type, and duration of stress to balance cell survival and death through an unknown mechanism. Recently, changes in the physical property of Hsf1 condensates due to persistent stress have been suggested to trigger apoptosis, highlighting the importance of biological phase separation and transition in cell fate decisions [1,2]. In this study, the mechanism underlying Hsf1 droplet formation and oxidative stress response was investigated through synchrotron-radiation circular dichroism (SRCD) spectroscopy [3].

SRCD spectra of droplets by Hsf1 WT and Hsf1 CS5 (cysteine-to-serine) mutant were measured at HiSOR BL-12. A 50-μm ultrathin cell and a detector right behind the cell were combined to eliminate the impact of the light scattering from turbid sample solutions including the droplets. The α-helical content was calculated from the SRCD spectra using the BeStSel program [4].

Disulfide bonds often stabilize protein structures. We hypothesized that the structural effects of Hsf1 disulfide bonds alter the intermolecular interactions. To evaluate the secondary structure of Hsf1 in the droplets, we used SRCD. The SRCD spectra of the Hsf1 WT droplet formed in the presence of dextran without the reductant showed minimum ellipticity at 207 nm, characteristic of high α-helical content (Figure 1a). In contrast, the negative ellipticity in the 205–230 nm region decreased in the Hsf1 CS5 droplet. BeStSel analysis showed that the α-helical content was 24.4% in WT and 13.2% in CS5, indicating that disulfide bonds stabilized the helical structure of Hsf1 in the droplet. The α-helical content in the Hsf1 WT droplet showed good agreement with the calculated α-helical content of 28.4%, as estimated from the Alphafold2 model including α-helices in the DBD, LZ1–3, and LZ4 (Figure 1b). Given the frequent appearance of transient helical structures in intrinsically disordered proteins and those involved in LLPS [5], these results suggest that secondary structure formation in the disordered region can be a strategy to regulate droplet properties in response to environmental change.

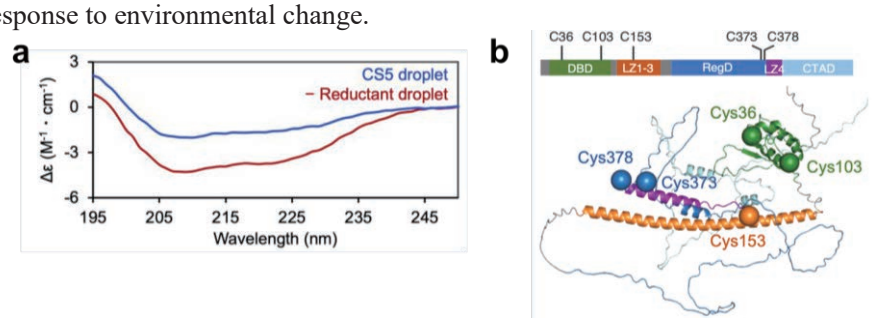


**FIGURE 1.** (a) SRCD spectra of 40 μM each of Hsf1 WT and CS5 in the presence of 18.75% (w/v) dextran 200. (b) Alphafold2 model of Hsf1 WT.

## REFERENCES

1. G. Gaglia, *Nat. Cel. Biol.,* **22**,151–158 (2020).
2. H. Zhang, et al., *Nat Cel Biol*., **24**, 340–352 (2022).
3. S. Kawagoe, et al., *JACS Au.* **5**, 2, 606–617 (2025).
4. A. Micsonai, et al., *PNAS*, **112** (24), E3095-E3103 (2015).
5. M. Arai, *Phys. Rev.*, **10**, 163–181, (2018).

# Dissecting Protein Folding Reaction by Synchrotron-Radiation Circular Dichroism

Munehiro Kumashiro[a], Soichiro Kawagoe [a], Koichi Matsuo[b], and Tomohide Saio[a]

[a]*Institute of Advanced Medical Sciences, Tokushima University*
[b]*Research Institute for Synchrotron Radiation Science, Hiroshima University*

**Keywords:** protein folding, circular dichroism.

Protein folding is a fundamental process in which an extended polypeptide chain forms a unique three-dimensional structure to perform its biological functions. Far-ultraviolet circular dichroism (far-UV CD) spectroscopy has been used as a powerful technique to investigate protein folding reactions [1]. However, urea, one of the most widely used chemicals for unfolding proteins, exhibits significant absorption in the far-UV wavelength region, which restricts the information obtainable from CD data. In this study, we used synchrotron radiation CD (SRCD) spectroscopy, which uses highly brilliant SR as a light source, to overcome this limitation. We investigated the secondary structure of a protein in the presence and absence of urea to characterize the unfolding of the protein.

Maltose-binding protein (MBP) was used as a folding model. The CD spectra of MBP in the presence and absence of 6 M urea were measured using a commercial CD spectrometer (J-1500, Jasco) and SRCD spectrometer at HiSOR BL-12.

Figure 1a shows the far-UV CD spectra of MBP, measured using a commercial CD spectrometer. Native MBP exhibited CD peaks characteristic of an α-helix structure, but the peak intensities of MBP with urea decreased, suggesting that urea denatured MBP. Note that the CD spectrum of MBP with urea below 208 nm was not observable due to the weak transmitted light. In contrast, as shown in figure 1b, the SRCD spectrum of MBP with urea showed a negative CD peak at 200 nm, which is characteristic of a random coil. This clearly indicates that MBP unfolded under urea conditions. Together, these data suggest that SRCD spectroscopy can be applied to characterize protein (un)folding reactions even under urea conditions. Recently, time-resolved SRCD spectroscopy has been developed [2]. Using this novel technique, it is important to investigate transient states of protein refolding reactions.

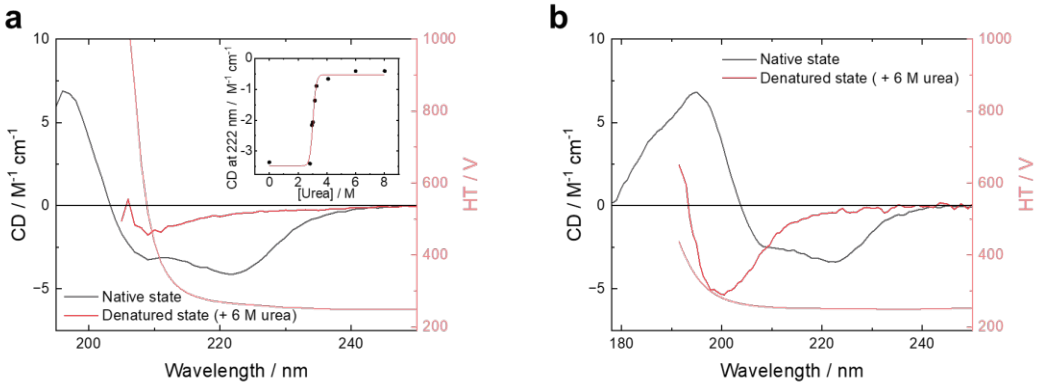


**FIGURE 1.** CD spectra of MBP in the presence and absence of 6 M urea, measured using a commercial CD spectrometer (a) and SRCD spectrometer (b). The high-tension voltage in the presence of 6 M urea is also shown in the same figures. The inset of fig. 1a shows the dependence of urea concentration on the CD intensity at 222 nm.

## REFERENCES

1. N. J. Greenfield, *Nat. Prot.* **1**,2891–2899 (2007).
2. S. Hashimoto and K. Matsuo, *Anal. Chem.* **96**, 26, 10524–10533 (2024).

# Structural Dynamics of $\alpha_1$-Acid Glycoprotein in the Membrane Interaction Revealed by Time-Resolved Vacuum-Ultraviolet Circular Dichroism

Satoshi Hashimoto[a] and Koichi Matsuo[a,b,c]

[a]*Graduate School of Advanced Science and Engineering, Hiroshima University, 1-3-1 Kagamiyama, Higashi-Hiroshima 739-8526, Japan*
[b]*Research Institute for Synchrotron Radiation Science, Hiroshima University, 2-313 Kagamiyama, Higashi-Hiroshima 739-0046, Japan*
[c]*International Institute for Sustainability with Knotted Chiral Meta Matter (WPI-SKCM2), Hiroshima University, 2-313 Kagamiyama, Higashi-Hiroshima 739-0046, Japan*

**Keywords:** Circular dichroism, $\alpha_1$-Acid Glycoprotein, Membrane interaction, Secondary structures

$\alpha_1$-acid glycoprotein (AGP) binds to drugs such as steroid hormones and releases them through membrane interactions, inducing its β-α structural transition[1]. Thus, AGP is used as a model protein for drug transport into the cell membrane. Studies have shown that two α-helices in the N- and C-terminal regions are key interaction sites[2,3] but the detailed membrane interaction mechanism, including electrostatic and hydrophobic forces, remains unclear. Recently, we developed a time-resolved (TR) vacuum-ultraviolet circular dichroism (VUVCD) spectrophotometer using synchrotron radiation to observe hierarchical protein structural transitions[4]. This study employed TR-VUVCD to analyze AGP's structural transitions and membrane interactions. TR-VUVCD spectra of AGP interacting with DMPG liposomes were measured within a 260–180 nm wavelength and 1–700 seconds (FIGURE 1). Analysis of TR data revealed that 90% of AGP's β-α transition occurred within 10 seconds of mixing with liposomes. Additionally, two distinct rate constants indicated that the transition from the native (N-) state to the membrane-bound (M-) state proceeded via an intermediate (I-) state. Secondary structure contents, segments, and sequences of AGP in the N-, I-, and MB-states were calculated from spectra. Physical parameters of each helical segment suggested that in the first step, two helices in the N-state interacted with the membrane, forming three new helices (I-state), and in the second step, an additional helix formed on the membrane (M-state). These insights provide valuable information for understanding AGP's drug delivery mechanism.

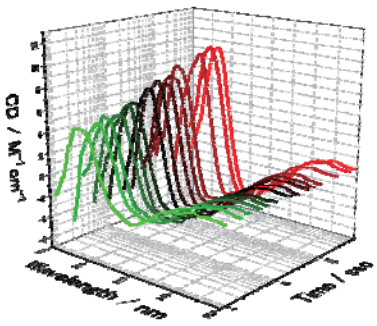


**FIGURE.** TR-VUVCD data sets in the interaction process between AGP and DMPG liposome.

## REFERENCES

1. K. Nishi, T. Mayumura, HB. Halsall, T. Handa, M. Otagiri, *Biochemistry* **43**, 10513-10519 (2004)
2. K. Matsuo, H. Namatame, M. Tanighchi, K. Gekko, *Biochemistry* **48**, 9103-9111 (2009)
3. K. Matsuo, K. Kumashiro, K. Gekko, *Chirality* **32**, 594-604 (2020)
4. S. Hashimoto and K. Matsuo, *Anal. Chem.* **96**, 10524-10533 (2024)

# Monitoring the Self-Assembly of Alginate Hydrogel Using Circular Dichroism

Tatsuki Haga[a], Masaya Yoshida[a], Takeharu Haino[a], Koichi Matsuo[b] and Mohamed I.A. Ibrahim[b]

[a]*Graduate School of Advanced Science and Engineering, Hiroshima University.*
[b]*Hiroshima Synchrotron Radiation Center (HiSOR), Hiroshima University, 2-313 Kagamiyama, Higashi-Hiroshima, Hiroshima 739-0046 Japan.*

**Keywords:** Alginate, Hydrogel, Self-Assembly, CD, AFM

Circular dichroism (CD) spectroscopy, traditionally used for studying the secondary structure of proteins and peptides [1], has not been yet established for studying polysaccharides (PSs). The current study has explored the potential of using CD in structural changes associated with PS hydrogelation. Certain PSs can change from a liquid to a gel when exposed to light, ions, or temperature. Alginate, an ecofriendly and nontoxic PS used in medicine and food, is especially known for forming hydrogels when mixed with polyvalent ions [2]. In the food industry, alginate serves as an additive to enhance texture and shape. This function is closely related to the conformational changes during sol-gel transitions, so structural analysis of alginate is helpful for maximizing its function as an additive.

Herein, CD experiments were carried out to investigate the structural changes associated with gel formation in the presence and absence of metal ions. Monovalent ions such as $Na^+$, $K^+$, and $Li^+$ didnot induce hydrogel formation, whereas hydrogels were obtained by divalents (e.g., $Ca^{2+}$, $Ba^{2+}$, $Cu^{2+}$, and $Zn^{2+}$), as well as trivalent ion (e.g., $Fe^{3+}$). The cations exhibited different influences on the native conformation of alginate, suggesting variations in the assembly of the alginate chains in the presence of different ions. Additionally, discrepancies in CD spectra reflected that the formed hydrogels possessed diverse mechanical, physical properties, and morphology.

The formulation of hydrogels is an evidence of the self-assembly phenomeneon. Alginate chains are interconnected, forming a cross-linked 3D-network structure that entraps water molecules, leading to hydrogel formation. The current work aimed to construct the self-assembly/gel phase diagram based on the CD observations. Concentration-dependent experiments, varying alginate concentrations or polyvalent ion concnetrations (i.e., $Ca^{2+}$), were conducted using a CD spectrometer. The concentration of the polyvalent ion that causes no change in the CD spectrum of alginate was marked as the initiation of aggregation, indicating that self-assembly of alginate chains was terminated (**Figure 1**, left). Thus, a $Ca^{2+}$ concentration of 1.56 mM, at 1.0 mg/ml alginate concentration, is referred to the transition concentration from the self-assembly to aggregation which is followed by hydrogel formation (**Figure 1**, right). This finding was reinforced by atomic force microscopy (AFM) imaging, which showed increased cross-linking and thichness of fibers at higher $Ca^{2+}$ concentration (2.5 mM) (**Figure 2**).

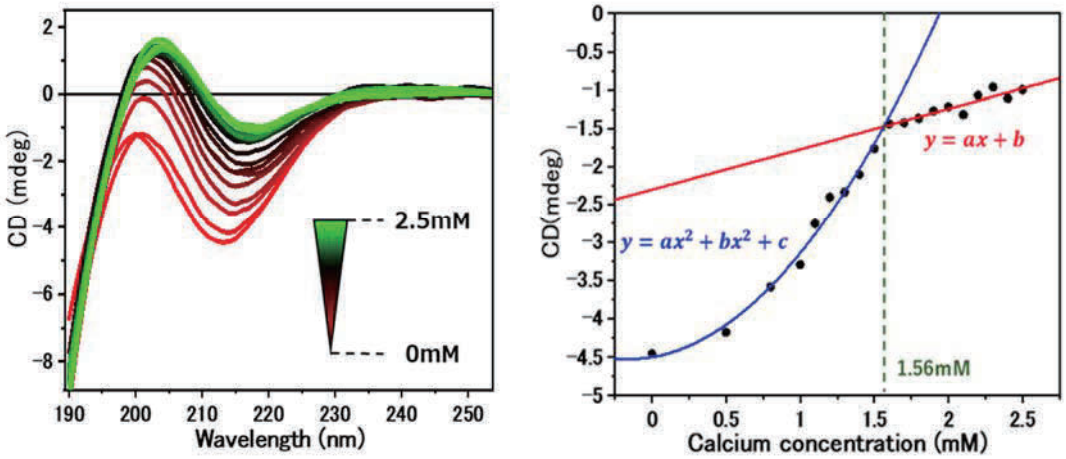


**FIGURE 1.** CD spectrum of alginate (1.0 mg/ml) as a function of $Ca^{2+}$ concentrations (0.5 mM ~ 2.5 mM) (left), and self-assembly transition diagram based on CD observations (right).

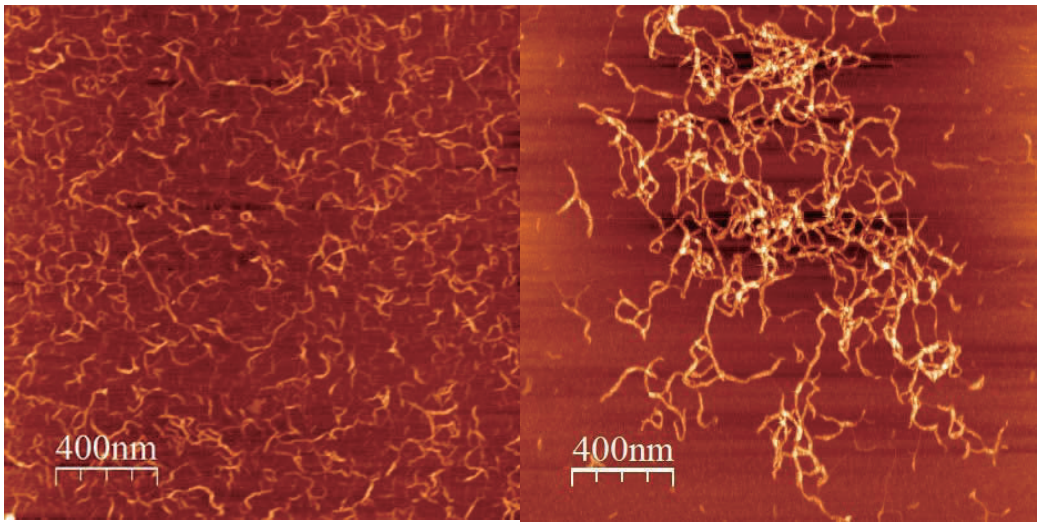


**FIGURE 2.** AFM images of the alginate-$Ca^{2+}$ system with [alginate] = 1.0 mg/ml and $Ca^{2+}$ concentrations of 1.0 mM (left), or 2.5 mM (right).

Ongoing investigations are underway to further explore the alginate-$Ca^{2+}$ hydrogel system using CD, aiming to study the kinetics and thermodynamics of hydrogelation process.

## REFERENCES

[1] K. Matsuo, G. Kunihiko, *Bulletin of the Chemical Society of Japan,* 2013, **86**, 675-689.
[2] J. Brus, M. Urbanova, J. Czernek, *Biomacromolecules,* 2017, **18**, 2478–2488.

# Structural and Conformational Studies of Peptide-based Hydrogels: Influence on Self-Assembling

Mohamed Ibrahim[a,b], Jacques Bodiguel[b], Marie-Christine Averlant-Petit[b], and Koichi Matsuo[a]

[a]*Hiroshima Synchrotron Radiation Center (HiSOR), Hiroshima University, 2-313 Kagamiyama, Higashi-Hiroshima, Hiroshima 739-0046 Japan.*
[b]*Université de Lorraine, CNRS, LCPM, F-54000 Nancy France.*

**Keywords:** Self-Assembly, Azapeptides, Hydrogels, Circular Dichroism.

Self-assembly is a captivating phenomenon within supramolecular chemistry, triggering the formation of hydrogels stabilized by non-covalent interactions including hydrogen bonding, π-π stacking, electrostatic interactions, and hydrophobic forces. Supramolecular gels-based low molecular weight molecules find applications in tissue engineering, drug delivery, biosensing, and catalysis [1]. Azapeptides, characterized by their nitrogen atoms, offer unique functionalities and stability, rendering them ideal for the fabrication of supramolecular hydrogels [2, 3]. In this study, two hydrogelator molecules derived from azapeptide family were designed, and structurally elucidated using various spectroscopic techniques. NMR, FTIR, UV-Vis, fluorescence, SEM, and rheology experiments were conducted to explore molecular, supramolecular, mechanical features. In solution, both molecules exhibit monomeric states adopting β-turn conformation stabilized by intramolecular hydrogen bonding, while the supramolecular structure (as revealed by X-ray crystallography) is stabilized mainly through intermolecular hydrogen bonding and π-π stacking (data is not shown). In the gel state, circular dichroism (CD) spectroscopy, is crucial for understanding the secondary structure and self-assembly of azapeptide-based hydrogels [4]. This study sheds light on the conformational changes occurring during the self-assembly process. For example, the temperature dependent experiment revealed the gel-sol transition associated with conformational changes (see **Figure 1**). By integrating principles from supramolecular chemistry, innovative azapeptide design strategies, and sophisticated spectroscopic methodologies, the development of functional hydrogels with tailored properties for diverse applications becomes achievable.

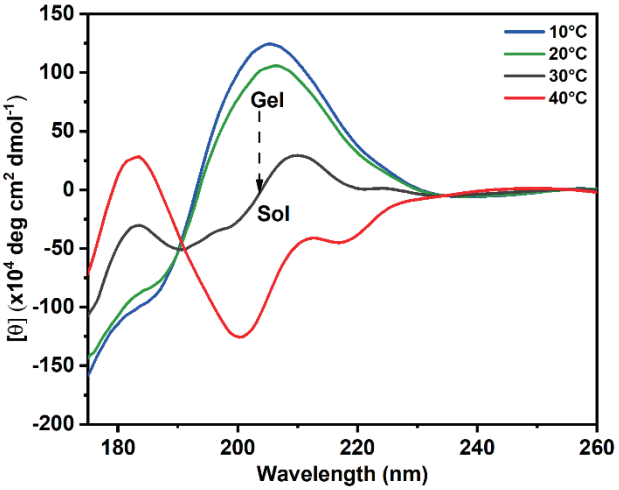


**FIGURE 1.** Temperature-dependent SRCD spectrum of azapeptide hydrogel (c = 0.8 w/w%, pH = 7.0).

## REFERENCES

1. M. J. Webber, E. A. Appel, E. W. Meijer, R. Langer, *Nature Materials*, 2016, **15**, pp. 13–26.
2. F. Rodríguez-Llansola, B. Escuder, J.F. Miravet, *Chemical Society Reviews*, 2015, **44**, pp. 6058–6071.
3. E. R. Draper, M. Wallace, S. Ladame, *Chemical Society Reviews*, 2020, **49**, pp. 7134–7171.
4. N. Berthet, P. Dugourd, R. Antoine, S. Lecomte, *Chirality*, 2019, **31**, pp. 458–476.
5. M. I. A. Ibrahim, G. Pickaert, L. Stefan, B. Jamart-Grégoire, J. Bodiguel, M.-C. Averlant-Petit, *RSC Advances*, 2020,**10**, pp. 43859-43869.

# Exploring the Conformational Dynamics of Peptide-Based Hydrogels and their Influence on Self-Assembly

Mohamed Ibrahim[a], Paul Hoschtettler[b], Loïc Stefan[b], Marie-Christine Averlant-Petit[b], and Koichi Matsuo[a]

[a]*Reserach Institute for Synchrotron Radiation Science (HiSOR), Hiroshima University, 2-313 Kagamiyama, Higashi-Hiroshima 739-0046 Japan.*
[b]*Université de Lorraine, CNRS, LCPM, F-54000 Nancy France.*

**Keywords:** Peptide-based hydrogels; Nucleopeptides; Self-assembly; Synchrotron radiation circular dichroism

Understanding the conformation and structural organization of peptide-based hydrogels is essential because their self-assembly determines mechanical strength, stability, and biological performance, which are critical for applications such as drug delivery and tissue engineering [1]. Previous work by the French team from Lorraine University introduced co-assembling nucleopeptides with complementary nucleobase moieties to enhance self-assembly and hydrogel properties. When mixed, the nucleopeptides p(TG)-FEFK and p(AC)-FEFK exhibited strong synergistic effects, improving hydrogel stiffness by over 2700-fold and stress resistance by more than 37-fold compared to single or mismatched systems. The hydrogel is stabilized through π-stacking and hydrogen bonding, leading to dense fibrillar networks that organize into highly porous hydrogel scaffolds capable of entrapping water [2].

In this study, Synchrotron Radiation Circular Dichroism (SRCD) was employed for its high sensitivity and extended spectral range to monitor real-time conformational changes during gelation. A 15 mM nucleopeptide mixture was prepared in 50 mM PBS (pH 7.0) by dissolving AC-FEFK (3.33 mg) and TG-FEFK (3.14 mg) in 300 µL buffer, followed by gentle warming (70 °C, 3 min) and pH adjustment. SRCD spectra were collected at BL-12 (HiSOR, Hiroshima University) using a 10 µm pathlength cell over 175–300 nm, with time-dependent measurements from 0–300 min.

Time-dependent SRCD revealed key structural transitions. For simplicity, **Figure 1** presents two representative CD spectra corresponding to the solution and gel states. At 20 min (solution state), the spectrum displayed a positive peak at 186 nm and two negative bands at 198 and 208 nm, features indicative of a disordered or partially folded conformation.

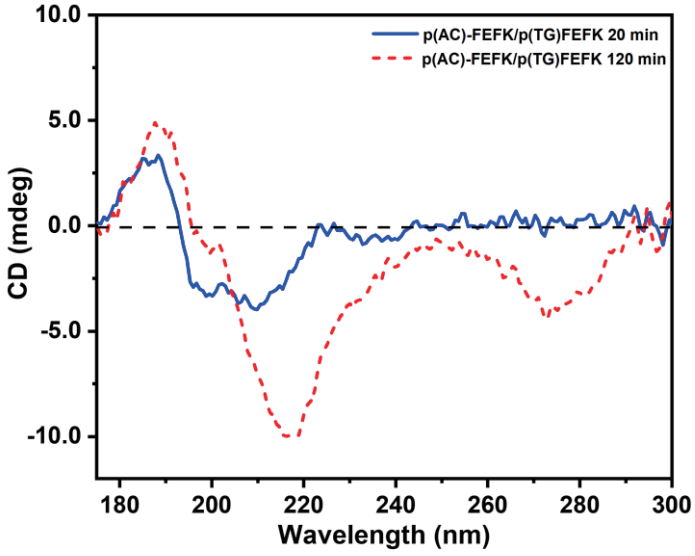


**FIGURE 1.** SRCD spectra of the complementary nucleopeptide mixture [p(TG)-FEFK / p(AC)-FEFK] at 15 mM in 50 mM PBS (pH 7.0) recorded during time-dependent measurement.

After 120 min (gel state), a red-shifted positive peak near 190 nm and an intense negative band at 217 nm emerged, indicating β-sheet-like structure formation. Additionally, a broad negative band at 274 nm appeared in the gel, reflecting π–π stacking between complementary nucleobases (A/T and C/G), confirming their role in stabilizing the supramolecular network. This hierarchical assembly, from peptide β-sheets to nucleobase interactions, underpins hydrogel formation.

These findings emphasize SRCD as a powerful tool for capturing subtle structural evolution during hydrogel assembly. Future studies will address the kinetics and thermodynamics of gelation under optimized conditions to further elucidate nucleopeptide-driven self-assembly mechanisms.

## REFERENCES


1. K. Fu, H. Wu, and Z. Su, *Biotechnol. Adv.* **49**, 107752 (2021).
2. P. Hoschtettler, G. Pickaert, A., M.-C. Averlant-Petit, and L. Stefan, *Chem. Mater.* **35**, 4259−4275 (2023).

# Secondary Structural Changes of The Oncoprotein NCYM Caused by Low Molecular Weight Inhibitors Using Vacuum-Ultraviolet Circular Dichroism

Tatsuhito Matsuo[a], Kazuma Nakatani[b,c], Daisuke Muto[b,c], Yusuke Suenaga[b], Taro Tamada[d,e], Agathe Nidriche[f], Judith Peters[f,g,h], and Koichi Matsuo[i]

[a]*Department of Medical Radiology, Faculty of Health and Medical Sciences, Hiroshima International University, Hiroshima, Japan*
[b]*Laboratory of Evolutionary Oncology, Chiba Cancer Center Research Institute, Chiba, Japan*
[c]*Graduate School of Medical and Pharmaceutical Sciences, Chiba University, Chiba, Japan*
[d]*Institute for Quantum Life Science, National Institutes for Quantum Science and Technology, Chiba, Japan*
[e]*Graduate School of Science and Engineering, Chiba University, Chiba, Japan*
[f]*Univ. Grenoble Alpes, CNRS, LiPhy, 38000 Grenoble, France*
[g]*Institut Laue-Langevin, 71 avenue des Martyrs, 38042 Grenoble Cedex 9, France*
[h]*Institut Universitaire de France, Paris, France*
[i]*Research Institute for Synchrotron Radiation Science, Hiroshima University, Japan*

**Keywords:** *de novo* protein, secondary structure, circular dichroism, cancer

NCYM is a Homininae-specific protein of 109 residues and the first *de novo* gene product that has been shown to have oncogenic functions [1]. It promotes metastasis in various tumors through interaction with other proteins such that NCYM is a promising therapeutic target. However, since NCYM is a *de novo* protein and thus its amino acid sequence is different from that of any protein known so far, there existed no structural information on NCYM. To gain structural information on NCYM, we have utilized vacuum-ultraviolet circular dichroism (VUVCD), which provides the secondary structure information on proteins in solution.

Previously (#18BU010), we investigated the structure of NCYM alone in solution by VUVCD and have revealed that some secondary structure components are concentrated in the center of the NCYM molecule while other parts are flexible [2]. The flexible nature of NCYM has been corroborated by our later studies using SAXS and NMR [3, 4].

In this beamtime, we studied the influence of the NCYM inhibitors, CCA-1.1, Lysine acetate, Bergenin, and X5636, and three types of SNPs (N52S, L63P, and V71D) on the structure of NCYM. The following samples were prepared and measured at 298 K:

| | | |
|---|---|---|
| #1 NCYM Wild-type (V70) | 2.5 mg/ml | |
| #2 NCYM Wild-type (V70) | 2.5 mg/ml + Acetate Lysine | 3 mM |
| #3 NCYM Wild-type (V70) | 2.5 mg/ml + CCA-1.1 | 62.5 μM |
| #4 NCYM Wild-type (V70) | 2.5 mg/ml + Bergenine | 200 μM |
| #5 NCYM Wild-type (V70) | 2.5 mg/ml + X5636 | 200 μM |
| #6 NCYM N52S | 2.1 mg/ml | |
| #7 NCYM L63P | 2.3 mg/ml | |
| #8 NCYM V71D | 2.1 mg/ml | |

The chemical composition of the buffer was 20 mM Phosphate buffer (pH 6.1), 100 mM NaF, 0.1 mM EDTA, and 0.1 mM PMSF.

Secondary structure analysis was carried out based on the measured spectra using SELCON3 program in combination with neural network algorithm [5, 6]. Preliminary analysis has shown that upon binding of CCA-1.1, residues 14-17 weaken the α-helicity while residues 91-94 strengthen the α-helicity. On the other hand, these regions took random coils upon binding of other three compounds. These results indicate that the residues 14-17 and 91-94 are involved in binding of the compounds employed, and that the higher affinity for NCYM of the three compounds than CCA-1.1 is related to disappearance of α-helices in the region. Differences in the secondary structure between SNPs are also detected, but detailed analysis is currently underway.

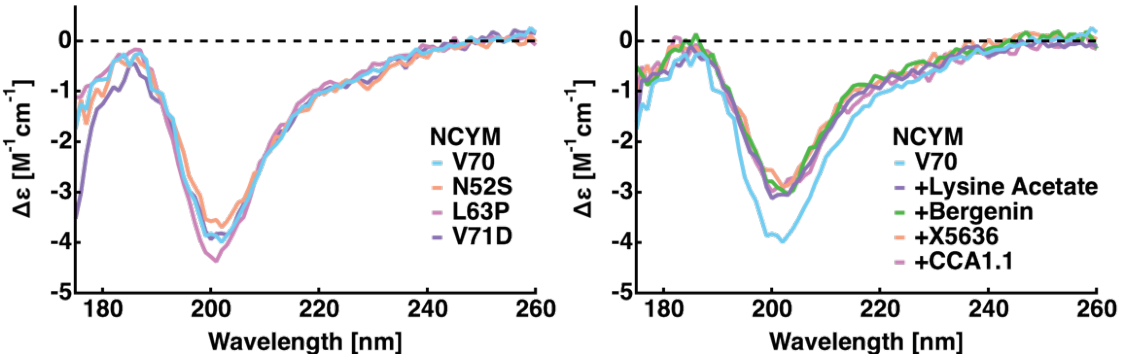


**FIGURE 1.** The measured VUVCD spectra of NCYM with/without low molecular weight inhibitors. (*Left*): Spectra of the wild-type (V70) and three variants with SNPs. (*Right*): Spectra of V70 in the absence or presence of low molecular weight inhibitors.

## REFERENCES

1. Suenaga, Y. et al., PLoS Genetics **10**, e1003996 (2014).
2. Matsuo, T. et al., Front. Oncol. **11**, 688852 (2021).
3. Yamamoto, S. et al., Front. Oncol. **13**, 1213678 (2023).
4. Mouhand, A. et al., Biomol. NMR Assign. **18**, 65-70 (2024).
5. Sreerama, N. and Woody, R.W., Anal. Biochem., **287**, 252-260 (2000).
6. Matsuo, K. et al., J. Biochem., **138**, 79-88 (2005).

# Monitoring the Self-Assembly of Alginate Induced by Calcium Ions Using Circular Dichroism

Tatsuki Haga[a], Masaya Yoshida[a], Takeharu Haino[a], Koichi Matsuo[b] and Mohamed I.A. Ibrahim[b]

[a]*Graduate School of Advanced Science and Engineering, Hiroshima University.*
[b]*Research Institute for Synchrotron Radiation Science (HiSOR), Hiroshima University, 2-313 Kagamiyama, Higashi-Hiroshima, Hiroshima 739-0046 Japan.*

**Keywords:** Self-assembly, Hydrogel, Circular Dichroism, Phase diagram

Circular dichroism (CD) spectroscopy is a valuable technique for analyzing the secondary structures of proteins and peptides [1]. However, its application to polysaccharide structural studies remains limited. Therefore, evaluating the feasibility of CD spectroscopy for polysaccharide analysis is essential. The alginate (SA) polysaccharide is known to transition from liquid to gel when exposed to polyvalent ions [2]. This study used CD experiments to investigate the effect of calcium ions ($Ca^{2+}$) on the structural changes of SA during self-assembly and hydrogel formation.

In the absence of $Ca^{2+}$, the CD spectrum of SA exhibited a peak around 200 nm and a trough near 215 nm (**Figure 1a**). Both peak intensities and positions gradually changed with increasing $Ca^{2+}$ concentration. Additionally, CD spectra of dried samples closely resembled those of liquid samples, indicating minimal structural changes due to drying. By analyzing the peak intensities and positions in the CD spectra, a phase diagram illustrating self-assembly and aggregation phases was constructed (**Figure 1b**).

These findings agreed with FTIR, SAXS (data not shown), and AFM analyses. FTIR spectra exhibited red shifts and splitting of the carboxylate ($–COO^–$) band near 1600 $cm^{-1}$, indicating progressive cross-linking at an intermediate stage prior to gel formation. SAXS measurements revealed fiber aggregation at critical $Ca^{2+}$ concentrations, with a pronounced increase in cylinder radius observed between 2.0–4.0 mM. AFM imaging supported a three-phase model: initial nucleation with fibril formation at low $Ca^{2+}$ levels, aggregation into dense fibers at intermediate concentrations, and the development of a 3D entangled network during the gelation phase (SA > 6.0 mg/mL, $Ca^{2+}$ > 6.0 mM). These results highlight the potential of CD spectroscopy for analyzing structural changes in SA-$Ca^{2+}$ hydrogel system.

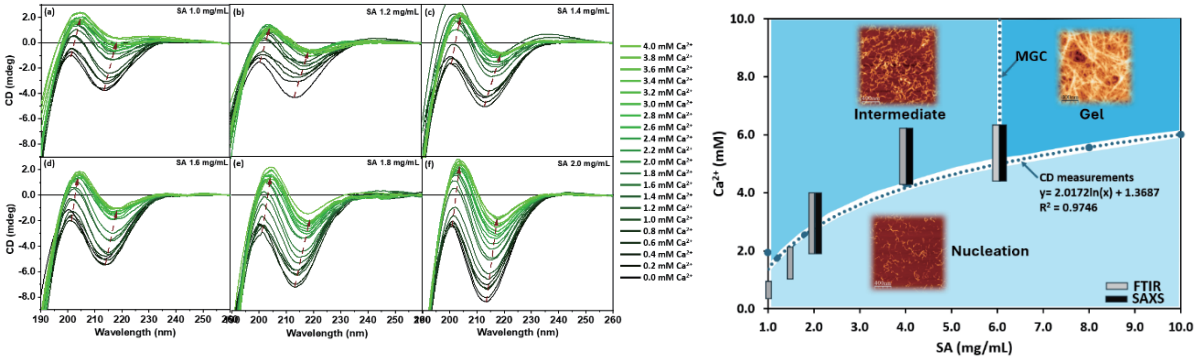


(a) (b)

**FIGURE 1.** (a) CD spectra during the assembly process (non-gel phase) of SA, at varying concentrations of SA and $Ca^{2+}$, and (b) proposed phase diagram of SA-$Ca^{2+}$ system based on CD findings.

## REFERENCES

1. K. Matsuo, G. Kunihiko, *Bull. Chem. Soc. Jpn.*, 2013, **86**, 675-689.
2. H. Wang, Y. Wan, W. Wang, W. Lia, and Jie Zhu, *Int. J. Food Prop.*, 2018, **21**, 1995-2006.

# Development of a Vertical Circular Dichroism Apparatus for Measuring Aggregated Biomolecules

Aoyama Kuya[1], Imaura Ryota[1], Hashimoto Satoshi[1], Haga Tastuki[1], Mohamed Ibrahim[2], Matsuo Koichi[1,2]

[1]*Graduate School of Advanced Science and Engineering, Hiroshima University*
[2]*Research Institute for Synchrotron Radiation Science, Hiroshima University*

**Keywords:** Circular Dichroism, Imaging

Circular dichroism (CD) measurements in the vacuum ultraviolet region (~140 nm) using synchrotron radiation are widely utilized for the precise structural and functional research of biomolecules in solutions. However, for solid and semi-solid biomolecules, such as amyloid fibrils which are causative materials of Alzheimer's disease, liquid-liquid phase separation involved in cellular and biological function regulation, and polymer hydrogels, accurate CD measurements are often difficult due to sample locality and anisotropy, which poses an obstacle to structural and functional research. Therefore, we developed a vertical circular dichroism apparatus and attempted to resolve these issues by using spatially resolved measurements with focused light from lenses and mirrors (which would address sample locality) and by introducing a new optical system [1] to resolve sample anisotropy.

As part of the performance evaluation of vertical apparatus, we measured the CD spectrum of camphor sulfonic acid solution, a standard CD sample, and confirmed an intensity ratio of 1:2 at 290 nm and 190 nm. Spatially resolved measurements were performed on the sample containing L- and D-alanine solutions, as well as on alginate gel sample. Although the resolution was low, the intensity and sign of circular dichroism depended on the position and types of samples. We will present the methods capable of removing sample anisotropy, comparing the conventional system.

## REFERENCE

1. G. E. Jellison and F. A. Modine "Two-modulator generalized ellipsometry: theory" *Appl. Opt.* **36**(31) 8190-8198 (1997).

# Hydration Structure of DMSO Probed by Concentration-Dependent ATR-UV Spectroscopy

Chika Sugahara[a], Koichi Matsuo[b], and Kazumasa Okada[a,b]

[a] *Graduate School of Advanced Science and Engineering, Hiroshima University, 1-3-1 Kagamiyama, Higashi-Hiroshima 739-8526, Japan*
[b] *Research Institute for Synchrotron Radiation Science, Hiroshima University, 2-313 Kagamiyama, Higashi-Hiroshima 739-0046, Japan*

**Keywords:** ATR-UV absorption spectra, hydration structure of DMSO

Hydration structure plays a fundamental role in the understanding of physical properties and chemical reactions of solutes in aqueous solutions. A solute of high affinity for water is dimethyl sulfoxide (DMSO), which has many applications in chemistry, biology, and pharmacy. Numerous physicochemical studies have been reported on the mixture, including thermochemical [1], nuclear magnetic resonance and infrared spectroscopic [2] studies. However, ultraviolet (UV) absorption spectra of the aqueous DMSO solution have hardly been reported so far, due to the strong absorption in this region.

In this study, we try to find the change of the hydration structure of DMSO by probing the variation of the UV absorption of DMSO. We particular focus on the n–σ* and n–π* absorption bands of DMSO because the n orbital has a character of the lone-pair electrons on the oxygen atom and these electrons are used to form a hydrogen bond with a hydrogen atom of surrounding water. The peak shift of the band is thus reflected by the change in the hydration structure of DMSO. Acquisition of the spectra having strong absorption requires a measurement technique called the attenuated total reflection (ATR) mode. We therefore introduce a new optical assembly consisting of a prism made of synthetic fused silica and a sample placement stage. This study becomes the first attempt to measure a series of UV absorption spectra of the aqueous DMSO solution as a function of concentration, as far as we know.

The experiments were performed on the beamline for vacuum-ultraviolet circular dichroism spectroscopy, BL-12. The chamber for measurements [3] was purged with a nitrogen gas flow. The absorption spectra were measured in the ATR mode with a prism made of synthetic fused silica (Edmund Optics Japan). All the spectra were recorded in the wavelength range of 180–280 nm, with a scan speed of 20 nm $min^{-1}$ and a sample interval of 2.0 s. The spectrum of liquid water was used as a reference. The sample solutions were prepared by mixing gravimetrically DMSO with water, with the molar fraction of DMSO ($x_D$) ranging from 0.025 to 0.125. The reagent DMSO was obtained commercially, and molecular sieves 3A 1/16 were immersed in it to prevent the liquid from contamination by moisture.

The ATR-UV spectra of the dilute DMSO solutions measured in this study show a significant change with concentration, as shown in Fig. 1. In particular, one can see an additional absorption band at ~ 240 nm coming up abruptly for the samples with $x_D$ = 0.100 and 0.125. Assignments of the bands are given based on the assignments for the UV spectrum of gaseous DMSO [4]: The peak at ~ 215 nm is assigned to the σ*(SO) ← n transition, that at ~ 195 nm to the π* ← π transition, and the peak at ~ 240 nm to the π* ← n transition. The appearance of the third band is indicative of the change in the hydration structure of DMSO.

Abrupt change is also seen in the position of the other peaks. The wavelength of the σ*(SO) ← n band changes between the samples of $x_D$ = 0.075 and 0.10, and that of the π* ← π transition changes between the samples of $x_D$ = 0.05 and 0.075. These facts also explain the change in hydration structure. We are concerned with the detection of stray light reflected from the prism installed, which needs to be examined carefully. We are planning to conduct this issue by introducing a light guide to our assembly.

We are grateful to the staff of the Research Institute for Synchrotron Radiation Science for stable operation of the storage ring.

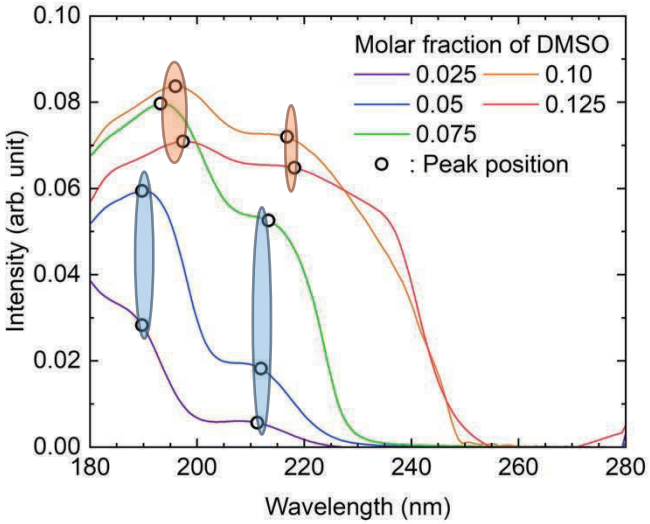


**FIGURE 1.** Absorption bands of DMSO in aqueous solutions. The open circles are the peak positions for samples with $x_D = 0.02–0.125$.

## REFERENCES


1. T. Kimura and S. Takagi, *Netsu Sokutei* **13**, 2–8 (1986).
2. K. Mizuno, S. Imafuji, T. Ochi, T. Ohta, and S. Maeda, *J. Phys. Chem. B* **104**, 11001–11005 (2000).
3. K. Matsuo, T. Funayama, R. Yonehara, H. Namatame, M. Taniguchi, and K. Gekko, *J. Electron Spectrosc. Relat. Phenom.* **144–147**, 1023–1025 (2005).
4. K. H. Sze, C. E. Brion, M. Tronc, S. Bodeur, and A. P. Hitchcock, *Chem. Phys.* **121**, 279–297 (1988).

# Validation of the foldability of the hydrophilic amino acid sequence

Naoki Tomita[a] , Riu Hirano[a], Leonard M.G. Chavas[a,b] and Yasufumi Umena[b]

[a] *Department of Applied Physics, Graduate School of Engineering, Nagoya University, Nagoya, Aichi 464-8602, Japan*
[b] *Nagoya University Synchrotron Radiation Research Center, Nagoya University, Nagoya, Aichi 464-8603, Japan*

**Keywords:** hydrophilic peptide, AlphaFold2

With the recent advent of AlphaFold2 [1], it has become possible to accurately predict the three-dimensional structures formed by natural proteins from their amino acid sequences. However, some studies have reported cases in which AlphaFold2 produces questionable predictions for amino acid sequences with properties not typically found in nature. One such case involves sequences that are fully hydrophilic and rich in threonine [2].

Protein folding is often driven by hydrophobic interactions, making the distribution of hydrophobic residues in the amino acid sequence critical for structure formation. However, AlphaFold2 has been shown to predict well-folded, unique structures even for fully hydrophilic, threonine-rich sequences lacking hydrophobic residues. Validation of such predictions is crucial for assessing the scope and limitations of AlphaFold2's applicability.

In this study, we focused on one such threonine-rich repeat sequence, composed of repeated TTTNKG units, which was previously predicted by AlphaFold2 to form an unique structure. To experimentally evaluate whether this sequence forms any secondary structure, we constructed a fusion protein composed of 15 tandem repeats of the TTTNKG unit, an N-terminal ubiquitin (UB) domain, and a purification tag, as illustrated in **FIGURE 1**. The UB domain was included as a soluble tag to enhance the expression stability of TTTNKG-repeat because repetitive peptide is generally hard to express. The construct (UB-triangle) was expressed in *Escherichia coli*, and purified using Ni-affinity chromatography.

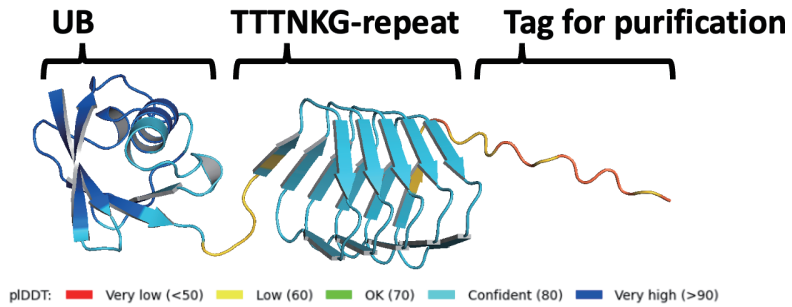


**FIGURE 1.** Depiction of the UB-triangle construct. Each residue is colored by the confidence score of AlphaFold2's structural prediction (plDDT).

We then conducted synchrotron radiation generated vacuum ultraviolet circular dichroism measurements using BL-12 at HiSOR to obtain the spectral data of UB-triangle. In addition, to isolate the CD spectrum of TTTNKG-repeat, we measured the spectrum of the UB domain alone under identical conditions. Each spectral data is shown in **FIGURE 2**. In **FIGURE 2C**, the difference spectrum—obtained by subtracting the concentration-normalized UB spectrum from the concentration-normalized UB-triangle spectrum—exhibits a prominent negative peak around 195 nm. This indicates that the TTTNKG-repeat adopts random coil conformations.

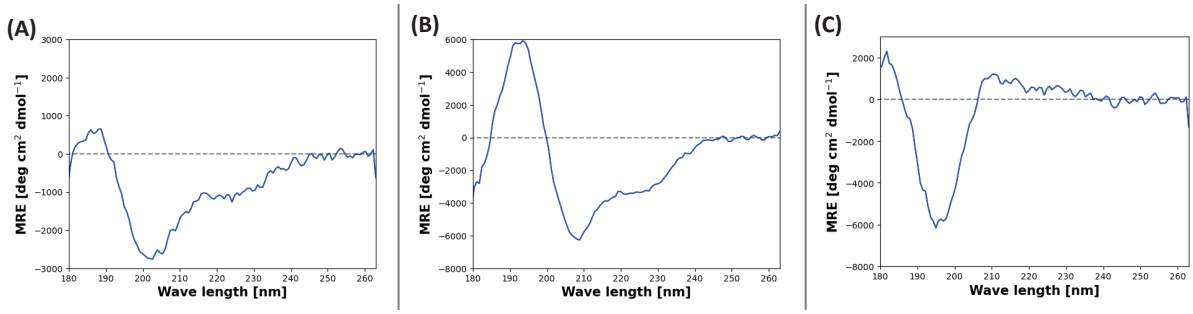


**FIGURE 2.** Spectrum plots of the mean residue ellipticity (MRE). (A) UB-triangle. (B) UB. (C) Difference between UB and UB-triangle.

These findings underscore that AlphaFold2 may not always accurately predict the structures of atypical amino acid sequences under physiological conditions. AlphaFold2 needs to be trained at giving a stable structure and, therefore, may not be a good tool when dealing with random coil structures. This study highlights the potential risks of relying blindly on AlphaFold2 predictions. Based on these results, we plan to investigate how the TTTNKG-repeat behaves structurally and dynamically in environments such as nonpolar solvents or under low-temperature conditions where entropic contributions vary from the physiological conditions.

## REFERENCES

1. J. Jumper *et al.*, *Nature*, **596**, 583-589 (2021).
2. N. Tomita, H. Onoda, L. M. G. Chavas, G. Chikenji, *Biophysics and Physicobiology*, **22**, e220005 (2025).

# Conformational analysis of H/D isotopically chiral compounds by circular dichroism spectroscopy

Haruna Tanno and Kawasaki Tsuneomi

*Department of Applied Chemistry, Tokyo University of Science, Kagurazaka, Shinjuku-ku, Tokyo 162-8601, Japan*

**Keywords:** Chirality, Isotope, Circular dichroism, Chiral isotopomer

We have previously reported the spontaneous absolute asymmetric Strecker synthesis from three achiral compounds—an aldehyde, an amine, and HCN—together with conglomerate formation of the resulting aminonitriles.[1,2] When aminonitriles were converted into diastereomeric isotopomers by introducing D/H chiral substitution, a solubility difference was observed between the *anti*- and *syn*-diastereomers, arising from hydrogen isotope asymmetry. Subsequent chiral amplification in the solid state enabled the stereoselective generation of aminonitriles with high stereoselectivity.[3]

The purpose of the present study is to investigate the origin of the slight solubility difference between diastereomeric isotopomers. To this end, the conformation of the chiral hydrogen isotopomers was analyzed by comparing experimental and theoretical CD spectra of the title compounds.

Hydrogen-isotopically chiral benzhydrylamines were dissolved in hexafluoro-2-propanol at a concentration of 5 mM. Chiral analysis of the enantiomeric isotopomers was performed using a vacuum ultraviolet circular dichroism (VUVCD) spectrometer. A $CaF_2$ cell (path length 50 μm) was used, and spectra were recorded in the range of 175–200 nm under a nitrogen atmosphere for both (*S*)- and (*R*)-enantiomers.

In conclusion, by utilizing the obtained CD spectra, conformational information of the chiral isotopomers will be derived through comparison with theoretical spectra.

## REFEARENCES

1. Kawasaki, T.; Takamatsu, N.; Aiba, S.; Tokunaga, Y. *Chem. Commun.* **2015**, *51*, 14377-14380.
2. Aiba, S.; Takamatsu, N.; Sasai, T.; Tokunaga, Y.; Kawasaki, T. *Chem. Commun.* **2016**, *52*, 10834-10837.
3. Kawasaki, T.; Kubo, H.; Nishiyama, S.; Saijo, T.; Yokoi, R.; Tokunaga, Y. *J. Am. Chem. Soc.* **2021**, *143*, 19525-19531.

# Structural study of proteins in skin tissue samples from humans aged 40s using scanning VUV-CD

*Ali Haider [1,2,3], Yusuke Kochi [1,2,3], Andrew K. Schulz [4], Kuya Aoyama[5], Koichi Matsuo [1,5], Aiko Sada [6,7,8], Hisako Sato [9], Elisabetta Matsumoto [1, 10], Malcolm Kadodwala [1,11] ,Katsuya Inoue [1,2,3]*

*[1] International Institute for Sustainability with Knotted Chiral Meta Matter (WPI-SKCM²), Hiroshima University, Higashihiroshima, 739-8526, Japan*
*[2] Department of Chemistry, Graduate School of Advance Science and Engineering, Hiroshima University, Higashihiroshima, 739-8526, Japan*
*[3] Chirality Research Center (CResCent) Hiroshima University, Higashihiroshima, 739-8526, Japan*
*[4] Haptic Intelligence Department, Max Planck Institute for Intelligent Systems, Stuttgart, Germany*
*[5] Research Institute for Synchrotron Radiation Science, Hiroshima University, Higashi-Hiroshima, Japan*
*[6] Division of Skin Regeneration and Aging, Medical Institute of Bioregulation, Kyushu University, Fukuoka, Japan*
*[7] International Research Center for Medical Sciences (IRCMS), Kumamoto University, Kumamoto, Japan*
*[8] Life Science Center for Survival Dynamics, Tsukuba Advanced Research Alliance (TARA), University of Tsukuba, Tsukuba, Japan*
*[9] Faculty of Science, Ehime University, 1 2-5, Bunkyo-cho, Matsuyama, Japan*
*[10] School of Physics, Georgia Institute of Technology, Atlanta, GA, 30332, USA*
*[11] School of Chemistry, Joseph Black Building, University of Glasgow, Glasgow G12 8QQ, U.K.*
*Author Email; d241619@hiroshima-u.ac.jp*
*haiderfiazali@gmail.com*

**Keywords:** Skin Aging, VUV-CD, Molecular Chirality

**Abstract**

Skin aging is a complex biological process involving structural and molecular alterations in extracellular matrix proteins, particularly collagen and elastin. In this study, we employed vacuum-ultraviolet circular dichroism (VUV-CD) spectroscopy at HiSOR to investigate age-related changes in the secondary structure and supramolecular chirality of human skin cell proteins. VUV-CD enabled access to deep UV transitions (below 190 nm), offering enhanced sensitivity to backbone conformations, especially in disordered and β-sheet-rich regions. Our comparative analysis across different age groups (late 30s to 40s) revealed a progressive decline in α-helical content and a corresponding increase in β-sheet and random coil features, suggesting age-induced peptide unfolding and destabilization. These spectral trends are consistent with previously observed patterns from QCL-based vibrational circular dichroism (QCL-VCD), which showed a loss of collagen triple-helix chirality and increased β-sheet signatures at ~1665 $cm^{-1}$. Together, the VUV-CD and QCL-VCD data indicate that molecular chirality degradation accompanies the structural disorganization of collagen fibers in aging skin. This integrated chiroptical approach provides a promising platform for non-invasive, spectroscopic evaluation of tissue aging and potential screening of regenerative therapies.

**Result**

The sample was a 30 μm thick section of dermis from a woman's abdomen, which was measured using VUV-CD. FIGURE 1 shows the mapping results at 230 nm for a sample from a 40-year-old person and the

absorption by position. Although a peak was expected at around 190 nm, no peak was observed in the measurement, and peaks of + or - were obtained around 230 nm to 240 nm (similar data was obtained for other samples). We also measured the ultraviolet region around 180 nm to 200 nm, but no characteristic peaks were obtained. The peaks obtained from the results are thought to originate from the triple helix structure of collagen molecules and collagen fibers, which are abundant in the dermis. However, multiple peaks were obtained at wavelengths different from those of absorption wavelengths originating from β-sheets or α-helices. There have been reports that when the structure of amyloid fibers changes, the CD absorption shifts toward higher frequencies, so we considered that a similar phenomenon may have occurred in this measurement. In other words, it is possible that multiple peaks were obtained due to structural diversification caused by the overlapping of multiple collagen fibers. We will investigate the amino acid sequence of this sample and perform further detailed analysis.

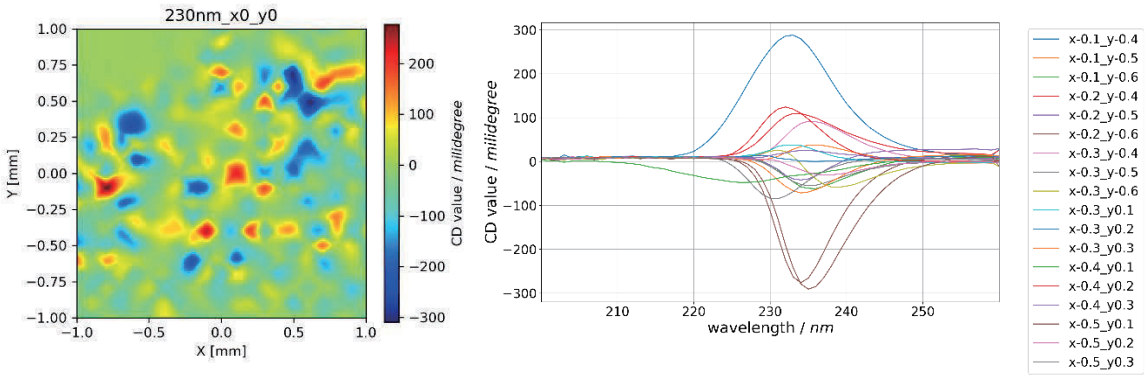


**FIGURE 1.** VUV-CD mapping at 230 nm(right), Absorption of VUV-CD by position(left)

## REFERENCES


1. Gekko, K., & Matsuo, K. (2006). Vacuum-ultraviolet circular dichroism analysis of biomolecules. Chirality, 18(5), 329–334.
2. Wallace, B. A., & Janes, R. W. (2001). Synchrotron radiation circular dichroism spectroscopy of proteins: Secondary structure, fold recognition and structural genomics. Current Opinion in Chemical Biology, 5(5), 567–571.
3. Barth, A. (2007). Infrared spectroscopy of proteins. Biochimica et Biophysica Acta (BBA) - Bioenergetics, 1767(9), 1073–1101.
4. Sreerama, N., & Woody, R. W. (2004). On the analysis of membrane protein circular dichroism spectra. Protein Science, 13(1), 100–112.
5. Iyer A, Roeters SJ, Kogan V, Woutersen S, Claessens MMAE, Subramaniam V. C-Terminal Truncated α-Synuclein Fibrils Contain Strongly Twisted β-Sheets. J Am Chem Soc. 2017 Nov 1;139(43):15392-15400.

# Fluorine substitution dependence of ultrafast electron transport in biphenyl monolayers induced by resonant core-excitations

Hayate Inoue[a], Kakuto Yoshioka[b], Shohei Asakura[b], Yuri Ohura[b], Shogo Tendo[b], Akinobu Niozu[c], and Shin-ichi Wada[a,b,d]

[a]*School of Science, Hiroshima University, Higashi-Hiroshima 739-8526, Japan*
[b]*Graduate School of Advanced Science and Engineering, Hiroshima University, Higashi-Hiroshima 739-8526, Japan*
[c]*Graduate School of Humanities and Social Sciences, Hiroshima University, Higashi-Hiroshima 739-8524, Japan*
[d]*Research Institute for Synchrotron Radiation Science, Hiroshima University, Higashi-Hiroshima 739-0046, Japan*

**Keywords:** Self-assembled monolayers (SAMs), Auger electron spectroscopy, Core-hole clock.

In recent years, the development of organic materials has attracted much attention in the field of electronic and optical devices. To realize industrial applications of organic materials, it is essential to optimize their electron transport properties and elucidate the correlation between molecular design and electron transport. For this reason, studies investigating the electron transport properties of various molecular systems have been actively conducted [1]. Among these studies, fluorine substitution has been suggested to control electron transport properties. So, we focused on a technique to investigate the electron transport properties of molecules by observing the Auger decay process with electron transport after resonant core-electron excitations using soft X-rays [2]. As a platform for this purpose, we focused on self-assembled monolayers (SAMs) where the end groups of molecules are located on the topmost surface of the substrate [3], which allows us to efficiently observe the electron transport from the end groups to the substrates. In this study, we investigated the effect of fluorine substituted positions on electron transport by measuring the intensity change of Auger electrons generated after soft X-ray irradiation for biphenyl SAMs with different fluorine substitution sites, as shown in Fig. 1.

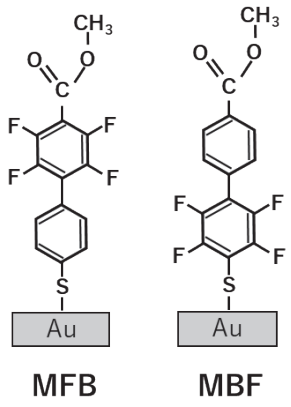


**FIGURE 1. Fluorine-substituted SAMs.**

Fluorine-substituted SAMs were prepared by immersing gold substrates in 1 mM ethanol solution of each sample for 24 hours and then rinsing with ethanol. Near-edge X-ray absorption fine structure (NEXAFS) and Auger electron spectroscopy (AES) measurements were performed on the prepared fluorine-substituted SAMs at HiSOR BL-13. NEXAFS measurements were performed in the carbon and oxygen K-edge regions, and the carbon K-edge region was measured in the angle range from 20° to 90° by changing the soft X-ray incidence angle by 10°. The π* peak was mainly observed at photon energies lower than the ionization threshold (IP), while the σ* peak was observed at higher photon energies. The MFB and MBF molecules were found to be oriented perpendicularly to the gold substrates.

AES measurements were performed not only on fluorine-substituted SAMs but also on insulating alkyl chain SAMs, where electron transport cannot occur. Fig. 2 shows the AES spectra excited at 532 eV, which is the excitation energy from the oxygen 1s orbital to the π*(C=O) orbital, where the resonant Auger decay

and electron transport processes compete. The AES spectra at 525 eV were used to subtract the photoelectron signal from the AES spectra at 532 eV. The AES spectra at 532 eV of fluorine-substituted SAMs shown as circles in Fig. 2 were well-reproduced as the red lines by fitting analysis using the linear combination of the pure resonant AES spectra of insulating alkyl chain SAMs (green lines) and the AES spectra of normal Auger decays, which is equivalent to Auger decay compete with electron transport (gray lines).

To quantitatively compare the electron transport processes, the analysis was performed using the core-hole clock method, which determines the electron transport time with respect to the core-hole lifetime $\tau_{core}$= 3.85 fs [4] for oxygen 1s from the fraction $P$ of the normal Auger component.

$$\tau_{CT} = \tau_{CH} \frac{1-P_{CT}}{P_{CT}}. \quad (1)$$

The electron transport times $\tau_{CT}$ were 15.7 ± 0.4 fs for MFB and 16.8 ± 0.4 fs for MBF, indicating that electron transport in MFB is about 1 fs faster. To discuss the results, we performed first-principles calculations of the lowest unoccupied molecular orbitals (LUMOs) involved in electron transport and found no clear difference in the LUMO shapes of the two molecules that could explain the difference in electron transport time. Since the molecular orbitals of the chemisorbed species are expected to change due to orbital hybridization with the Au substrate, a detailed understanding of each molecule would be obtained by performing first-principles calculations that consider the effect of the Au substrates.

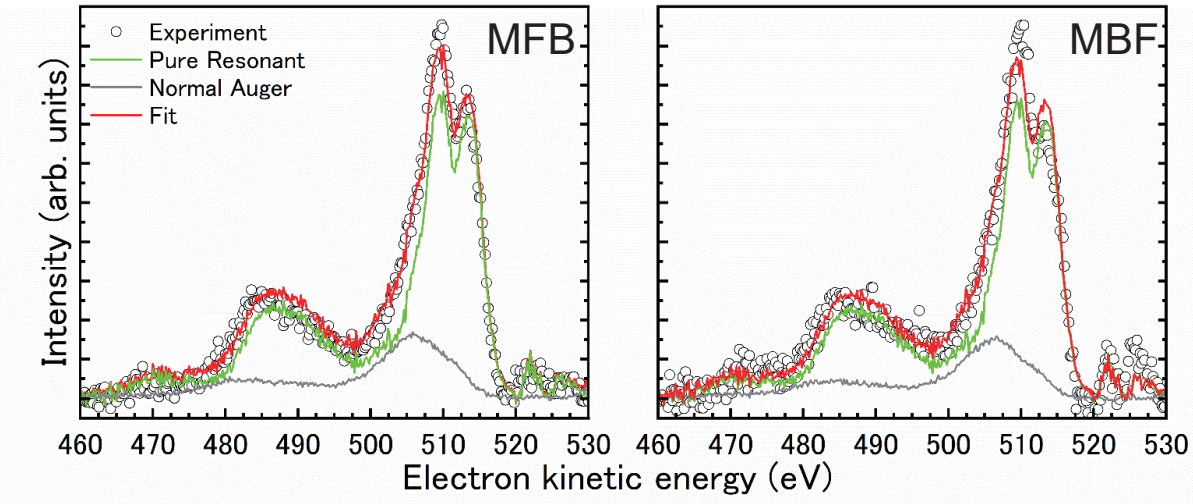


**FIGURE 2. AES spectra (white circles) of MFB (left) and MBF (right). The fitted lines (red) are obtained by linear combination of the resonant Auger components (green) and the electron transport components (normal Auger, gray).**

## REFERENCES


[1] R. L. Carroll and C. B. Gorman, Angew. Chem., Int. Ed. **41**, 4378 (2002).
[2] M. Zharnikov, Acc. Chem. Res. **53**, 2975 (2020).
[3] J. C. Love, L. A. Estroff, J. K. Kriebel, R. G. Nuzzo, and G. M. Whitesides, Chem. Rev. **105**, 1103 (2005).
[4] C. Nicolas and C. Miron, J. Electron Spectrosc. Relat. Phenom. **185**, 267 (2012).

# DFT calculations for NEXAFS analysis measured for organic molecules

Shohei Asakura[a], Genki Hashimoto[b], Yuri Ohura[a], Shogo Tendo[a], Kakuto Yoshioka[a], Akinobu Niozu[c], and Shin-ichi Wada[a,b,d]

[a] *Graduate School of Science and Engineering, Hiroshima University, Higashi-Hiroshima 739-8526, Japan*
[b] *Faculty of Science, Hiroshima University, Higashi-Hiroshima 739-8526, Japan*
[c] *Graduate School of Humanities and Social Sciences, Hiroshima University, Higashi-Hiroshima 739-8526, Japan*
[d] *Research Institute for Synchrotron Radiation Science, Hiroshima University 739-0046, Japan*

**Keywords:** NEXAFS (near edge X-ray absorption fine structure), DPPC, Phospholipids, DFT(density functional theory)

Density functional theory (DFT) is a powerful technique that allows theoretical predictions of electronic states and is also effective in interpreting X-ray absorption spectra (NEXAFS). However, proper implementation of DFT calculations requires setting parameters and mastering analysis techniques according to the characteristics of the target molecules. Gaining insights into the structure and order of molecular membranes, aggregates, is particularly challenging. Therefore, we focused on phospholipid molecules as the target molecules forming the molecular membranes and performed DFT calculations on these.

Phospholipids play a vital role in living organisms, especially in forming the basic structure of cell membranes. These membranes are not just physical barriers but also function as sites for information transmission and protein function regulation, deeply involved in fundamental biological activities. Therefore, understanding the structure and properties of cell membranes is crucial for elucidating biological processes. Recent research has advanced by forming biomimetic membranes supported on metal substrates to study their structure and properties. In this context, understanding the electronic structure of lipid membranes is essential, and DFT calculations have gained attention as one method for this analysis.

Additionally, the hydrocarbon chains of lipid molecules are desirable systems for the introduction of DFT calculations. Hydrocarbon chains in lipid molecules are generally composed mostly of saturated chains without carbon-carbon double bonds. This characteristic provides ideal conditions for implementing DFT calculations and is suitable for verifying whether the analysis technique is appropriate through comparison with experimental results. Therefore, in this study, we focused on the hydrocarbon chains of lipid molecules and reproduced NEXAFS spectra using DFT calculations to examine their effectiveness by comparing with experimental results.

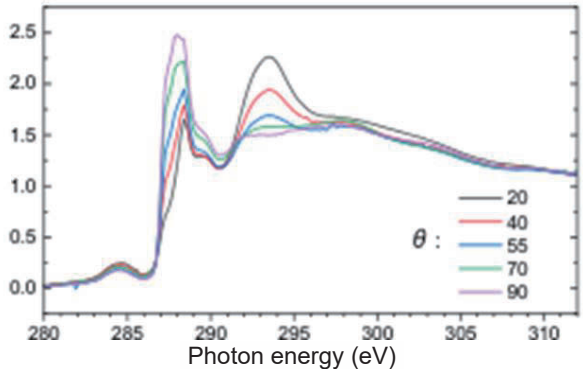


**FIGURE 1.** Carbon K-edge NEXAFS spectra of DPPC phospholipid membranes supported on metal substrates obtained from experiments. θ represents the angle between the irradiated soft X-ray and the substrate. The intensity of the spectra changes with θ, indicating orientation dependence.

The carbon K-edge NEXAFS spectra of phospholipid membranes supported on metal substrates obtained from previous studies are shown in Fig. 1. Strong polarization dependence at 288 eV and 293 eV can be observed in these spectra. Previous studies attributed this polarization dependence to the hydrocarbon chains that significantly contribute to the order of the molecular membranes and discussed the orientation and order of the phospholipid membranes on metal substrates. In this study, to verify the transitions attributed in previous studies, we focused on the hydrocarbon chains of DPPC as shown in Fig. 2(a) and assumed a model molecule as shown in Fig. 2(b). Calculations were performed on this molecule, with the superscript letters of each carbon atom representing the labeling used in the spectrum calculation. This model molecule includes carbons thought to be related to the orientation of the lipid membrane. The calculation results of this model molecule allow the decomposition of the soft X-ray absorption spectra of phospholipids into each carbon atom. This information is expected to provide detailed insights into the spectra.

In the actual calculations, we performed structural optimization of the model molecule using DFT calculations, followed by reproducing the NEXAFS spectra using the TP method, which calculates the energy difference between the ground state and the excited state of the obtained structure. Gaussian16 was used for structural optimization with DFT calculations. The functional used was B3LYP, and the basis set was 6-31G. StoBe/Demon was used for TP method calculations.

Fig. 3 shows the NEXAFS spectra obtained from calculations for each carbon atom, together with the experimental result (top in the figure). Since the energy obtained from calculations differs from the experimental results, the calculated energy was calibrated so that the main peak originating from $C^1$ aligns the main peak of the experiment attributed to π*(C=O) (green broken line). The main peak appearing at lower energy than this broken line was found to consist of three peaks originating from aliphatic chain carbons and one peak originating from carbonyl carbon, based on a comparison with the calculations. That is, this component composed of π*(C=O) and σ*C-H at $C^4$, $C^6$, $C^7$, and $C^8$ in the aliphatic chains. The component on the high-energy side of the green dashed line consists of contributions from carbon atoms adjacent to electronegative oxygen or carbonyl carbon, such as $C^2$, $C^3$, and $C^4$. Based on this information, it is possible to perform fitting analysis of experimental results that separate the head group, carbonyl group, and aliphatic chain of lipid molecules, enabling more detailed analysis of the phase structure of lipid membranes.

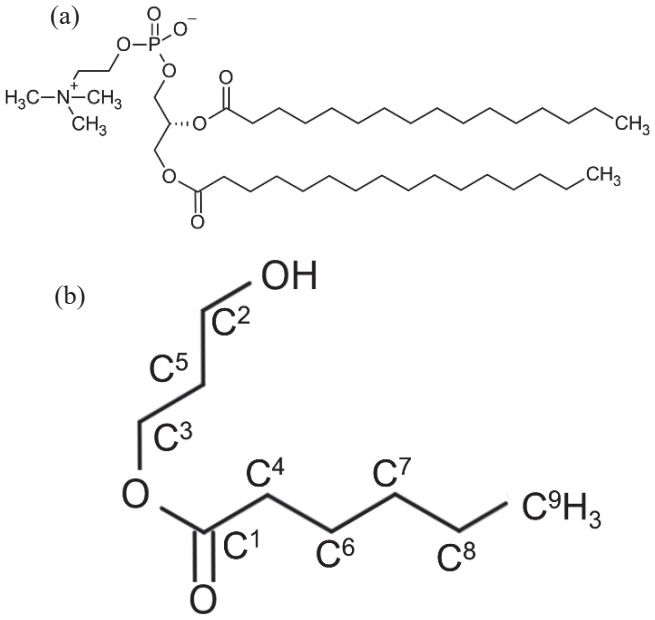


**FIGURE 2.** Structural formulas of (a) DPPC phospholipid and (b) the model molecule used for DFT calculations. The superscript letters of each carbon atom represent the labeling used in the calculations.

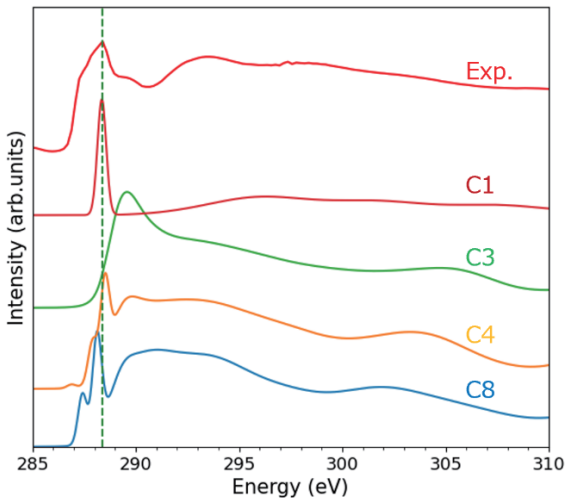


**FIGURE 3.** Comparison between the NEXAFS spectra obtained from this DFT calculations and experimental result.

# Determination of organic molecular film thickness on gold substrates using soft X-ray photoelectron spectroscopy

Shogo Tendo[a], Kakuto Yoshioka[a], Akinobu Niozu[b], Shohei Asakura[a], Yuri Ohura[a], and Shin-ichi Wada[a,c]

[a]*Graduate School of Advanced Science and Engineering, Hiroshima University, Higashi-Hiroshima 739-8526, Japan*
[b]*Graduate School of Humanities and Social Sciences, Hiroshima University, Higashi-Hiroshima 739-8524, Japan*
[c]*Research Institute for Synchrotron Radiation Science, Hiroshima University, Higashi-Hiroshima 739-0046, Japan*

**Keywords:** Self-assembled monolayers (SAMs), X-ray photoelectron spectroscopy (XPS), Thickogram analysis.

Self-assembled monolayers (SAMs) enable nanoscale surface functionalization by taking advantage of molecular design flexibility, and are expected to have a wide range of applications including electronic devices, catalysts, biosensors, and solar cells [1]. The electronic conductivity, surface energy, and reactivity of SAMs vary significantly depending on molecular film thickness and orientation. Therefore, precisely determining these structural properties is essential for the design and application of SAMs. In this study, we determined the molecular film thickness using X-ray photoelectron spectroscopy (XPS) and evaluated its validity based on molecular orientation angles determined by near-edge X-ray absorption fine structure (NEXAFS) spectroscopy and structural optimization through density functional theory (DFT) calculations.

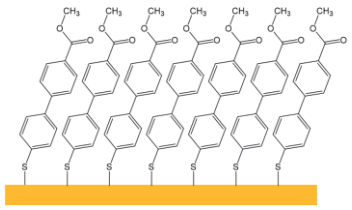

**FIGURE 1.** Graphical image of MBP SAM.

The experiments were conducted at HiSOR BL-13, a bending magnet beamline suitable for analyzing surfaces composed of light elements. The target samples were SAMs formed by chemisorption via thiol groups onto gold substrates, consisting of six different molecules with varying aromatic backbone structures, each terminating in a methyl ester group. In this study, the methodology for determining film thickness is presented using biphenyl (MBP) SAMs as an example, as shown in Fig. 1. A wide-scan XPS spectrum of MBP SAMs, acquired with a hemispherical electron energy analyzer at a photon energy of 396 eV, is shown

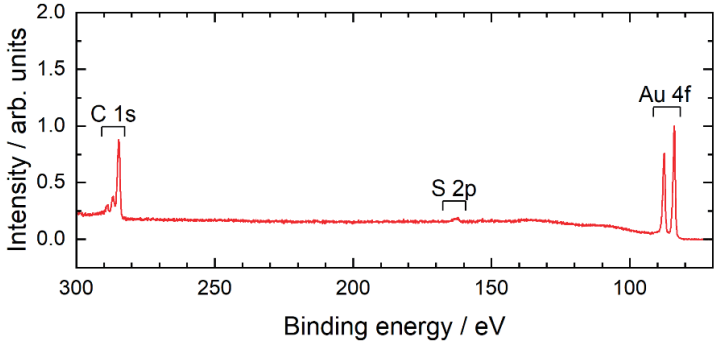


**FIGURE 2.** Wide-scan XPS spectrum of MBP SAM. The spectrum was acquired at a photon energy of 396 eV, with the intensity normalized to the Au $4f_{7/2}$ peak.

in Fig. 2.

Since photoelectrons undergo inelastic scattering within the molecular film, the intensity of the Au 4f photoelectron peak, $I_{Au}$, is expressed by the equation

$$I_{Au} = s_{Au}\exp(-t/\lambda_{Au}\cos\theta). \quad (1)$$

Similarly, the intensity of the C 1s photoelectron peak, $I_C$, is given by the equation

$$I_C = s_C\exp(-t/\lambda_C\cos\theta), \quad (2)$$

where $t$ represents the molecular film thickness and $\theta$ is the emission angle (0° in this study). And $\lambda_{Au}$ and $\lambda_C$ denote the inelastic mean free paths (IMFPs) of Au 4f and C 1s photoelectrons, respectively, while $s_{Au}$ and $s_C$ represents their corresponding detection sensitivities. The sensitivity ratio of $s_{Au}$ / $s_C$ was determined using hexadecanethiol SAM of known molecular film thickness (17.3 Å) [2]. Based on these equations (1) and (2), Cumpson derived the Thickogram equation for film thickness determination using XPS [3].

$$\ln\left(\frac{I_C\, s_{Au}}{I_{Au}\, s_C}\right) = \ln\sinh\left(\frac{1}{2\lambda_C\cos\theta}\right) + \left[\left(\frac{E_C}{E_{Au}}\right)^{0.75} - \frac{1}{2}\right]\frac{t}{\lambda_C\cos\theta} + \ln 2 \quad (3)$$

The IMFP ratio was estimated using an empirical formula based on the ratio of kinetic energies: $\lambda_C/\lambda_{Au} = (E_C/E_{Au})^{0.75}$. Further data analysis was performed using the electron spectroscopy analysis software COMPRO12 [4], leading to the determination of an MBP SAM thickness of 14 Å.

The film thickness was estimated based on the determination of the molecular orientation angle using NEXAFS spectra and the calculation of molecular length via DFT. Fig. 3 shows the polarization-dependent NEXAFS spectra at the carbon K-edge. The absorption intensities of the π* peaks increased and those of the σ* peaks decreased when the angle of incidence of soft X-rays was varied from 20° to 90°. This dependence indicates that the molecules are oriented upright on the substrate. From the fitting analysis of the first peak with an excitation energy of about 285 eV to the π* orbital of the phenyl rings, the molecular orientation angle was determined to be 19°. The film thickness predicted from this orientation angle, the molecular length (12 Å) calculated using DFT (B3LYP/6-31G**), and the S–Au bond length (2.3 Å [5]) was 14 Å, which agreed with the result of Thickogram analysis. This agreement validates the method for determining the thickness of organic molecular films using XPS.

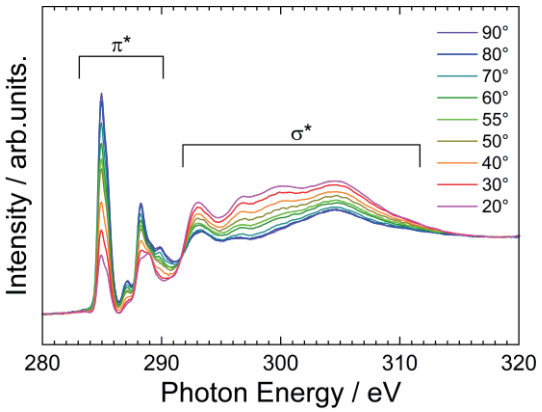


**FIGURE 3.** NEXAFS spectra of MBP SAM at the carbon K-edge. The polarization dependence was measured by varying the incident angle of soft X-rays from 20° (grazing incidence) to 90° (normal incidence) relative to the substrate.

Thickogram analysis was found to be applicable not only to SAMs on gold substrates but also to SAMs on nanoparticle surfaces [6]. This suggests that the method is a valuable tool for evaluating the thickness of organic thin films in fields requiring nanoscale molecular film control, such as electronic devices, catalysts, and biosensors.

## REFERENCES


[1] J. C. Love, L. A. Estroff, J. K. Kriebel, R. G. Nuzzo, and G. M. Whitesides, Chem. Rev. **105**, 1103 (2005).
[2] H. A. Biebuyck, C. D. Bain, and G. M. Whitesides, Langmuir **10**, 1825 (1994).
[3] P. J. Cumpson, Surf. Interface Anal. **29**, 403 (2000).
[4] K. Yoshihara, JSA **23**, 138 (2017).
[5] C. Battocchio, F. Porcaro, S. Mukherjee, E. Magnano, S. Nappini, I. Fratoddi, M. Quintiliani, M. V. Russo, and G. Polzonetti, J. Phys. Chem. C **118**, 8159 (2014).
[6] S. Tendo, A. Niozu, K. Yoshioka, M. Tabuse, J. Adachi, H. Tanaka, and S. Wada, Phys. Chem. Chem. Phys. **27**, 388 (2025).

# XAS/XMCD measurements in nanostructures converted from titanium oxide nanosheets

R. Kurogi[a], M. Sawada[b], and M. Hara[c]

[a]*Graduate School of Science and Technology, Kumamoto University, 2-39-1 Kurokami, Kumamoto 860-8555, Japan*
[b]*Research Institute for Synchrotron Radiation Science, Hiroshima University, 2-313 Kagamiyama, Higashi-Hiroshima 739-0046, Japan*
[c]*Faculty of Advanced Science and Technology, Kumamoto University, 2-39-1 Kurokami, Kumamoto 860-8555, Japan*

**Keywords:** 2D materials, titanium oxide nanosheet, anatase, defect, XAS, XMCD

Two-dimensional (2D) materials have attracted great interests not only in the fundamental physics but also in their potential future applications. In this study, we focus on nanostructures converted from titanium oxide nanosheets, one of the 2D oxide materials with thickness of about 1 nm. For the sample preparation, we deposited titanium oxide nanosheets chemically exfoliated from layered titanates [1] on highly doped Si substrates and then induced structural changes by the following two approaches. One is thermal annealing which leads to transformation from the lepidocrocite structure into anatase structure, which has been reported in previous studies [2,3]. The other is $Ar^+$ ion irradiation which introduces defects in the nanosheets. We carried out XAS/XMCD measurements for investigating the electronic and magnetic states in the titanium oxide nanostructures.

Figure 1 shows the XAS spectra at Ti *L* edge for the samples annealed at 900°C under various atmospheres. The peaks at the $L_3$ and $L_2$ edges corresponding to $Ti^{4+}$ slightly shift towards higher energy after the annealing. A splitting of $e_g$ peak at the $L_3$ edges disappears especially when annealed in vacuum. For all of the samples, we have not observed a distinct XMCD signal.

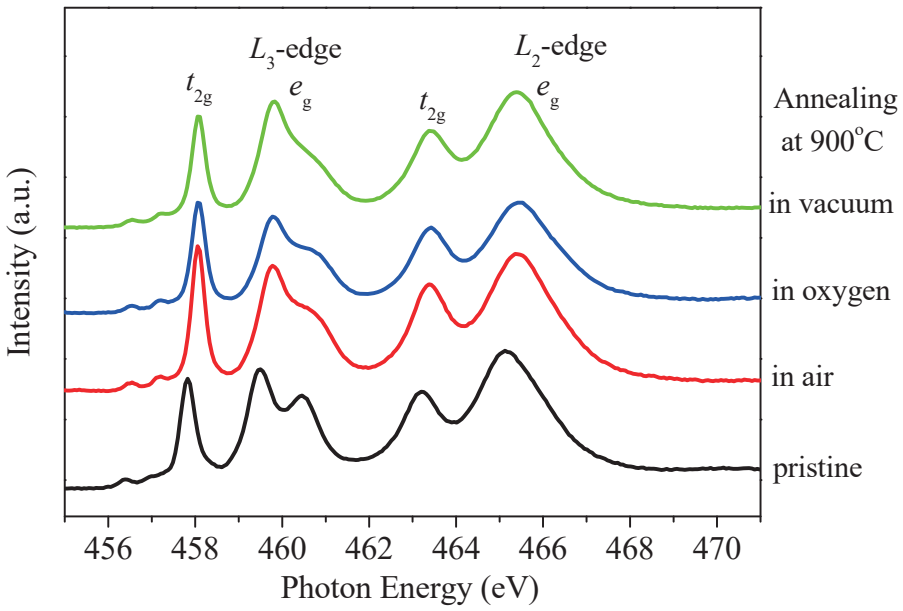


**FIGURE 1.** XAS spectra at Ti 2p→3d edge for the samples annealed at 900 °C in different atmospheres.

Figure 2 shows the XAS spectra at Ti *L* edge for the samples of titanium oxide nanosheets with different fluences of $Ar^+$ ion irradiation. $Ar^+$ ions with the acceleration voltage of 200 V were irradiated perpendicular to the plane of the sample. The changes in the XAS spectra are simlilar to those in the case of annealing shown in Fig. 1. There is no clear dependence on the irradiation fluence. In previous studies, the surface of a $TiO_2$ anatase film with a thickness of 40–150 nm was found to be ferromagnetic due to Ti defects induced by $Ar^+$ ion irradiation [4,5]. We also found a similar ferromagnetic behavior of titanium oxide nanosheets with $Ar^+$ ion irradiation by a SQUID magnetometory [6]. However, we have not detected a finite XMCD signal probably because the signal-noise ratio is insufficient to reveal the defect-induced ferromagnetic components in the extremly-thin titanium oxide nanosheets.

In summary, we have investigated the electronic and magnetic states in nanostructures converted from titanium oxide nanosheets. XAS spectra reveal the changes in the electronic states accompanying the transformation to anatase and the generation of defects. Further improvements for XMCD measurements are needed to obtain clear signals to elucidate the origin of defect-induced ferromagnetism in titanium oxide nanosheets.

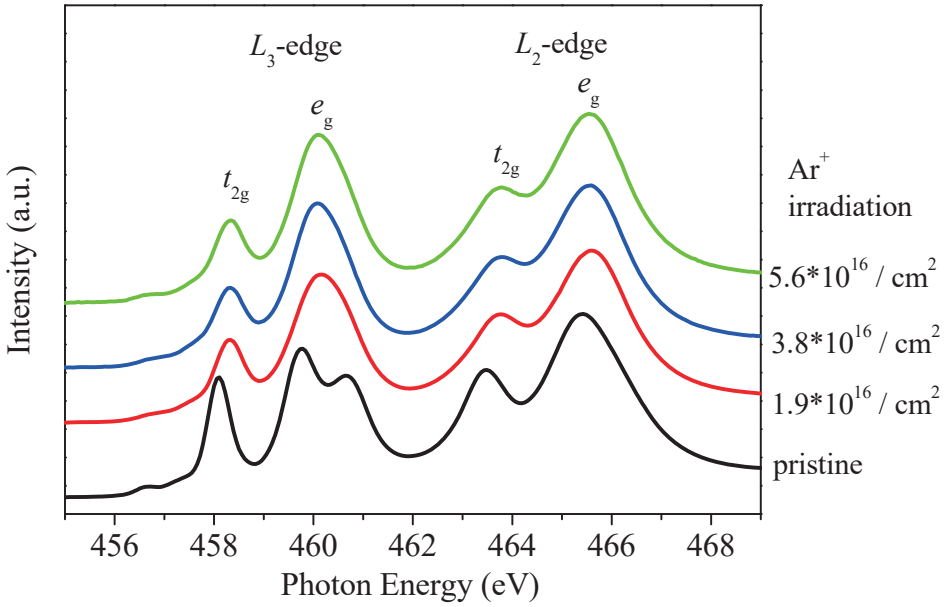


**FIGURE 2.** XAS spectra at Ti 2p→3d edge for the samples with different fluences of $Ar^+$ irradiation.

## REFERENCES


1. T. Tanaka, Y. Ebina, K. Takada, K. Kurashima and T. Sasaki, *Chem. Mater.* **15** 3564 (2003).
2. K. Fukuda, T. Sasaki, M. Watanabe, I. Nakai, K. Inaba and K. Omote, *Cryst. Growth Des.* **3** 281 (2003).
3. K. Fukuda, Y. Ebina, T. Shibata, T. Aizawa, I. Nakai and T. Sasaki, *J. Am. Chem. Soc.* **129**, 202 (2007).
4. M. Stiller, A. T. N'Diaye, H. Ohldag, J. Barzola-Quiquia, P. D. Esquinazi, T. Amelal, C. Bundesmann, D. Spemann, M. Trautmann, A. Chassé, H. B. Hamed, W. A. Adeagbo and W. Hergert, *Phys. Rev. B* **101** 014412 (2020).
5. L. Botsch, P. D. Esquinazi, C. Bundesmann and D. Spemann, *Phys. Rev. B* **104** 014428 (2021).
6. R. Kurogi, T. Sueyoshi, A. Funatsu, T. Yamauchi, Y. Hashimoto, A. Endo, T. Ichii, K. Hara, M. Sawada, M. Mizumaki and M. Hara, *Nanotechnology* **36**, 255702 (2025).

24BU016

# Raman microscopy of 18-crown-6 ether

Yuki Shiro[a], Yuka Horikawa[a] and Osamu Takahashi[b]

[a]*Graduate School of Sciences and Technology for Innovation, Yamaguchi University, Yamaguchi, Japan*
[b] *Research Institute for Synchrotron Radiation Science, Hiroshima University, Higashi-Hiroshima, 739-8526, Japan*

**Keywords:** 18-crown-6, Raman microscopy

Crown ethers are large cyclic chemical compounds that consist of a ring containing several ether groups and have the general formula $(\text{-}CH_2\text{-}CH_2\text{-}O\text{-})_n$. These compounds are the few molecular groups that encapsulate group 1 and 2 atoms and were discovered by C. J. Pederson, who was awarded the Nobel Prize in Chemistry in 1987 [1]. The incorporated metal cations can be controlled by changing the ring size and chemically modifying the functional groups. The discovery of crown ethers has become the foundation of the later concept of supramolecular science.

Although measurements of liquids using soft X-ray spectroscopy have become popular, there are few studies on crown ethers using this spectroscopy. To investigate the electronic states and cation inclusion behavior of crown ethers, Raman spectroscopy and soft X-ray absorption spectroscopy have been performed in acetonitrile (AN) as a solvent, which does not include an oxygen atom in the molecule. In this report, the results of the Raman spectroscopy are presented.

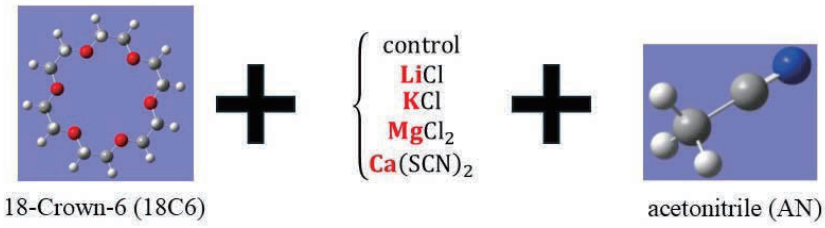


**FIGURE 1.** Molecular system in the present study.

18-Crown-6 (18C6) was used as a typical example of crown ether. It is known that 18C6 has a hole size of approximately 0.26 – 0.32 nm, which matches the size of the $K^+$ ion (0.28 nm), and is known to selectively encapsulate $K^+$ in aqueous solutions. In contrast in vacuum, another selectivity was observed [2]. The used metal salts were LiCl, KCl, $MgCl_2$, and $Ca(SCN)_2$. 18C6 melted at 40 °C was mixed with an equimolar amount of metal salt, and then AN was added to prepare a sample containing a single crystal (Fig. 2). Raman spectra were obtained for both the crystalline and liquid portions using Raman spectrometer (Mobile-RAM 300, Lambda-vision).

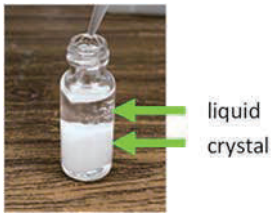


**FIGURE 2.** A sample used the experiment.

The results are summarized in Fig. 3. The peak at approximately 900 $cm^{-1}$ is due to AN. In contrast, the two peaks at 800 – 850 $cm^{-1}$ are due to 18C6 with $D_{3d}$ symmetry [2]. No peaks originating from 18C6 were measured in the liquid portion, whereas peaks from both the AN and 18C6 crystals were measured in the crystalline portion, demonstrating the separation of the liquid and crystalline portions.

In the 18C6/LiCl/AN system, the peak near 850 $cm^{-1}$ is slightly shifted to a higher wavenumber compared to that of the 18C6/AN system. This peak shift indicates that the ring structure is distorted when $Li^+$ ion is incorporated into the crown ether. The same peak shift was also observed for the 18C6/KCl/AN system. For the 18C6/$MgCl_2$/AN system, although the separation of the crystals and liquid could not be measured well, most of the signal was AN, and it appeared that the liquid portion was present. For the 18C6/$Ca(SCN)_2$/AN system, although the separation of the crystals and liquid could not be measured in the same manner as the 18C6/$MgCl_2$/AN system, $Ca^{2+}$ ions may be incapsulated in 18C6, because the observed peak is completely

different from the case of 18C6/AN.

Based on the above results, the cations examined in this study should be incapsulated in the crystalline portion. These results will be useful for future XAS measurements.

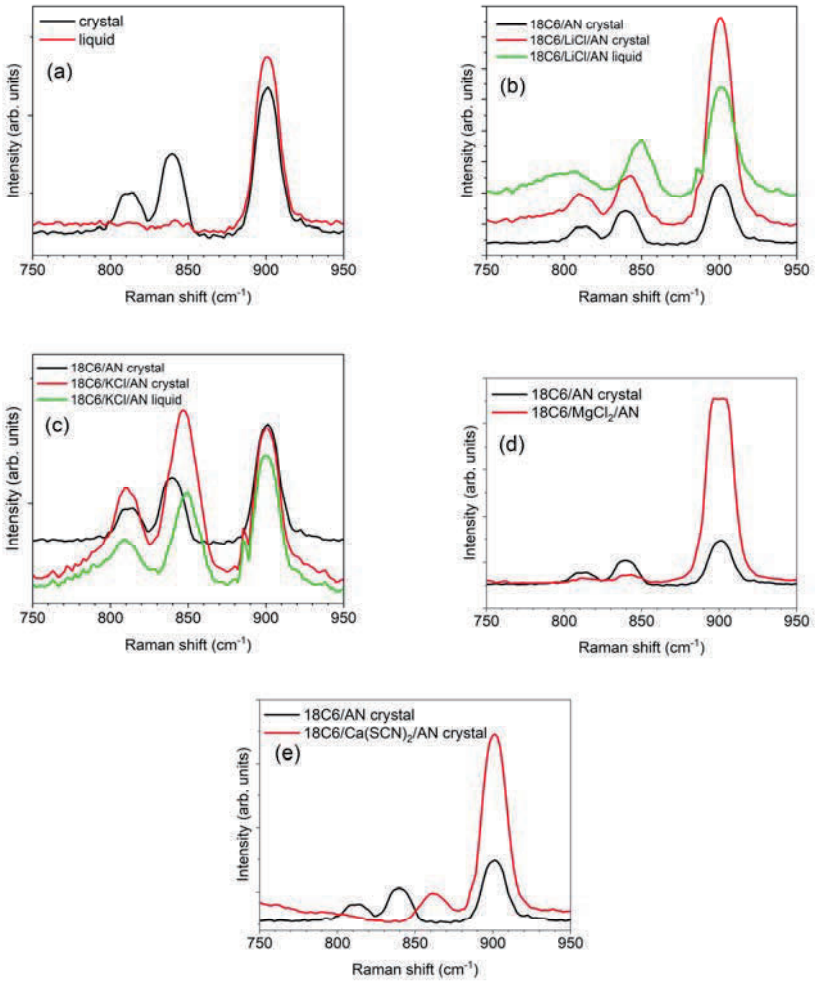


**FIGURE 2.** Raman spectra of (a) 18C6/AN system, (b) 18C6/LiCl/AN, (c) 18C6/KCl/AN, (d) 18C6/$MgCl_2$/AN, and (e) 18C6/$Ca(SCN)_2$/AN systems. For all panels spectra of 18C6/AN crystal form is also depicted.

## REFERENCES


1. C. J. Pederson, *J. Am. Chem. Soc.*, **89**, 7017-7036 (1967).
2. Z. F. Jing et al., *J. Mol. Liq.*, **311**, 113305 (2020).
2. H. Takeuchi et al., *J. Mol. Struct.*, **146**, 197-212 (1986).

24BU017

# Viscosity measurement of organic acid-base systems

Taichi Hirakawa[a], Yuka Horikawa[a] and Osamu Takahashi[b]

[a] *Graduate School of Sciences and Technology for Innovation, Yamaguchi University, Yamaguchi, Japan*
[b] *Research Institute for Synchrotron Radiation Science, Hiroshima University, Higashi-Hiroshima, 739-8526, Japan*

**Keywords:** Viscosity, Carboxylic acid, electrical conductivity.

Acetic acid (AcO) is a weak acid, so its degree of ionization is low, and the electrical conductivity of pure acetic acid is $3.8 \times 10^{-4}$ mS/cm. However, when acetic acid and 1-methylimidazole (1-MI, electric conductivity is $6.4 \times 10^{-2}$ mS/cm) are mixed, the electric conductivity of this solution increases to 8.0 mS/cm at concentrations of $\chi_{1\text{-MI}} = 0.15$ and 0.35. Because the solution was a mixture of acid and base, it was predicted that acetic acid would release $H^+$ and 1-MI would receive it, causing an increase in electrical conductivity. However, Raman spectroscopy studies have shown that acetic acid exists almost as a neutral molecule at a concentration of $\chi_{1\text{-MI}} = 0.5$ [1], and the number of ions is maximum at $\chi_{1\text{-MI}} = 0.25$, which is different from the maximum concentration of electrical conductivity. The above results suggest that, in addition to electrical conduction due to the movement of ionic molecules, a unique mechanism such as the Grotthuss mechanism, may occur in this mixture. To elucidate these phenomena, which cannot explain the standard mechanism of ion conduction, a measurement of the viscosity of these solutions is required in addition to a measurement of the number of ions.

The electrical conductivity σ of a dilute ionic system is proportional to the product of the ion concentration and inverse of the viscosity,

$$\sigma \propto [\mathrm{ion}]/\eta.$$

In the present study, measurements of electrical conductivity and viscosity were performed for a mixture of acetic acid and several bases, such as 1-MI, pyridine, N-methylpyrrolidine (NMP), and imidazole, to examine the behavior of the electrical conductivity curves depending on the $\Delta pK_a$ of the mixed solutions. The number of ions was estimated from the peak integral values obtained by Raman spectroscopy. The viscosity is measured using B-type viscometer (Toki Sangyo, Co. Ltd.).

The results are arranged in order of their $\Delta pK_a$ values (Fig. 1). As shown in Fig. 1(a), the acetic acid/pyridine mixture system, number of ions, viscosity, and electrical conductivity were maximized when the molar fraction of the base was approximately $\chi_{py} = 0.17$. Furthermore, viscosity was maximized at approximately the same concentration. In Fig. 1(b), the acetic acid/1-MI mixture system, the number of ions and viscosity were maximized approximately $\chi_{1\text{-MI}} = 0.25$, on the other hand, the electrical conductivity was maximized different concentrations, i.e., approximately $\chi_{1\text{-MI}} = 0.15$ and 0.35. As shown in Fig. 1(c), the acetic acid/NMP mixture system, the number of ions and viscosity are maximized at approximately $\chi_{NMP} = 0.30$, and the electrical conductivity is maximized in the region where the acid is more concentrated. As shown in Fig.1(d), the acetic acid/imidazolium mixture system, the viscosity was maximized at approximately $\chi_{IM} = 0.40$, on the other, and the electrical conductivity was maximized at approximately $\chi_{IM} = 0.20$ and 0.80.

For all mixtures, a correlation was observed between the increase in the number of acetic acid ions and the viscosity. It should be noted that the number of base ions also increases with increasing acetic acid ions owing to the acid-base mixture system, which is not shown in the figures. It may be considered that the increase in viscosity is due to the increase in Coulomb repulsion between positive/negative ions. Thus, it is speculated that for the acetic acid/IM mixture systems, the viscosity may be maximized at a comparable concentration at the maximum number of ions, which we did not measure the number of ions.

Next, we focused on the maximum ion concentration, that is, the mole fraction of the base. These values are 0.17, 0.25, 0.30, and 0.40 for acetic acid/pyridine, 1-MI, NMP, and imidazole, indicating that the mixture system with a smaller $\Delta pK_a$, that is, the more difficult it is to generate ions in a mixture, the more likely ions are generated in the acid concentration region. The more acid concentration region, the more number of

acidic clusters exist. It is thought that the present acid acts as a strong acid by forming dimers or chain clusters, making it possible to generate ions with the base. It has also been proposed that the Grotthuss mechanism uses a hydrogen-bonding network with dimers and chain clusters [2]. Considering this, it is highly likely that rapid $H^+$ conduction via the Grotthuss mechanism may occur in any mixed systems when the base molar fraction is in the range of 0.1 to 0.2, and the maximum value of the electrical conductivity can be also confirmed. Although the acetic acid/pyridine system was not explicitly visible in the electrical conductivity curve because the region in which the number of ions was maximized overlapped in the range of 0.1 to 0.2, it is possible that the Grotthuss mechanism is expressed in this system in the acid-rich regions. For the acetic acid/1-MI system, $\Delta pK_a$ was approximately 2, and double maxima of the electrical conductivity were observed. According to Watanabe et al. [2], double maxima may be observed by the Grotthuss mechanism. For the acetic acid/imidazole system, an additional maximum was observed at a mole fraction of approximately 0.8 is observed. According to Long et al. [3], imidazole itself forms chain clusters in the same way as acetic acid and causes proton hopping. Thus, in the case of this mixed system, it is considered that the second maximum occurs even in the base-rich region because of the fast conduction of $H^+$ ions utilizing the hydrogen-bonding network between the bases.

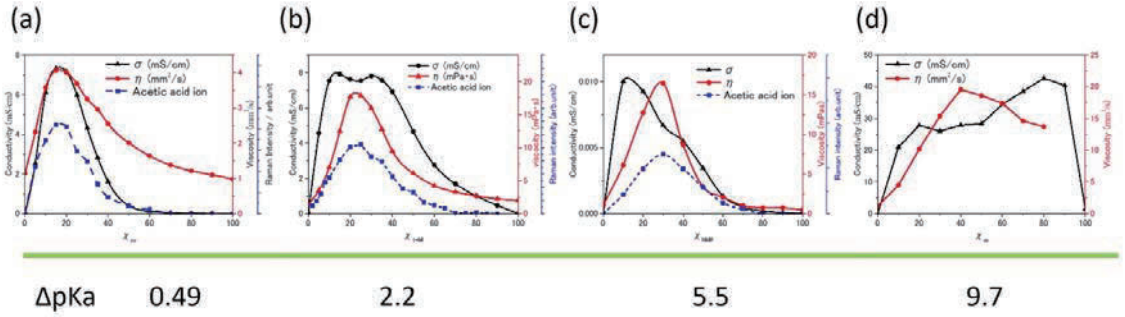


FIGURE 1. Electronic conductivity, viscosity, and number of ions of acetic acid ions as a function of concentration of base. (a) AcO/Pyridine, (b) AcO/1-MI, (c) AcO/NMP, and (d) AcO/Imidazole.

From the above measurements, the electrical conductivity curve for various acetic acid/several base mixture systems can be understood by both the number of ions Raman spectroscopy and the measurement of viscosity, which cannot be explained by the number of ions only. In the future, the mechanism of electrical conductivity will be elucidated, in addition to molecular dynamics simulations.

## REFERENCES

1. H. Doi *et al*., *Chem. Eur. J*. **19**, 11522 (2013).
2. H. Watanabe, *et al*., *J. Phys. Chem. B* **124**, 49, 11157‑11164 (2020).
3. Z. Long, *et al*., *J. Phys. Chem. Lett*. **11**, 15, 6156‑6163 (2020).

24BU018

# Model and XES calculations of organic and inorganic hybrid crystals

Osamu Takahashi[a], Shinnosuke Horiuchi[b], Go Watanabe[c,d], and Yoshihisa Harada[e]

[a] *Research Institute for Synchrotron Radiation Science, Hiroshima University, Higashi-Hiroshima, 739-8526, Japan*
[b] *Department of Basic Science, Graduate School of Arts and Sciences, The University of Tokyo, 3-8-1 Komaba, Meguro-ku, Tokyo 153–8902, Japan*
[c] *Department of Physics, School of Science, Kitasato University, 1-15-1 Kitazato, Minami-ku Sagamihara, Kanagawa 252-0373, Japan.*
[d] *Department of Data Science, School of Frontier Engineering, Kitasato University, 1-15-1 Kitazato, Minami-ku Sagamihara, Kanagawa 252-0373, Japan*
[e] *The Institute for Solid-State Physics, The University of Tokyo, Kashiwa, Chiba 277-8581, Japan*

**Keywords:** Resorcin[4]arene, Water, X-ray emission spectroscopy, density functional theory.

Water molecules at interfaces play critical roles in numerous natural phenomena and in the material sciences [1,2]. For example, water-mediated forces enable large biomolecules to form complex three-dimensional structures that are essential for biological activity, mediating ligand–receptor binding, enzymatic reactions, and material transport. Similarly, the water at the interface between the aqueous phase and both organic and inorganic materials affects the chemical and physical properties, influencing biomaterial adhesion, aqueous chemical reactions, water harvesting systems and clathrate hydrate formation. Visualizing the 3D alignment of water clusters and hydrogen-bonding networks on organic polymer surfaces at atomic resolution remains challenging. This difficulty stems from the complexity of tailoring polymer surface structures. Furthermore, analytical methods to characterize multilayered water channels have yet to be developed.

In our recent study, we obtained a unique supramolecular crystal **1•EtOH** composed of a flexible resorcin[4]arene and a rigid coordination complex salt *via* solid-state driven assembly. This supramolecular crystal possesses one-dimensional (1D) infinite pores within its crystal lattice and exhibits a solvent exchange reaction with water molecules through a single-crystal-to-single-crystal fashion. Upon solvent exchange, the crystal **1•$H_2O$** forms 1D water channels surrounded by the crystal framework. Thanks to the atomically well-resolved framework confirmed by X-ray crystallographic analysis, the hydrogen-bonding patterns of the water molecules and their inhomogeneity at the pore surfaces were elucidated through a combination study of X-ray diffraction studies, vibrational spectroscopy, X-ray emission spectroscopy (XES), and molecular dynamics (MD) simulations at atomic resolution [3]. In this study, we aim to investigate the theoretical aspects of water molecules in the 1D pore of the supramolecular crystal by XES simulations.

The XES calculations in a detail are shown below. Simulated XES spectra were obtained within the framework of the density functional theory. The basis sets and functionals were used as same as those reported previously [4,5]. The semiclassical Kramers-Heisenberg (SCKH) formula was applied to mimic the experimental XES spectra [4]. To correct entanglement of the potential energy curve and discontinuous of the transition moment, a new scheme with the genetic algorithm was applied [6]. The final calculated spectra were shifted by –2.8 eV to match the experimental result. Although the intensities of $1b_2$ and $3a_1$ peaks are overestimated in the calculations, the contributions for $1b_2$ and $3a_1$ peaks were not discussed.

The theoretical studies for structurally defined water clusters at the pore surface observed in the X-ray analysis were also evaluated. The structures for the calculations were built up, based on the X-ray results. The positions of oxygen atoms of the water molecules were fixed, and hydrogen atoms were added manually among the water molecules, then their geometry optimizations were performed using Gaussian 09 [7] using

ONIOM method [8]. In the present study, a two-layer ONIOM scheme was applied. Water molecules were treated using quantum mechanical (QM) methods with B3LYP/6-31G(d,p) level of theory, and the porous framework was applied using classical molecular mechanical (MM) methods with the universal force field (UFF). Geometries of the porous framework were fixed during the QM/MM scheme. One of the water molecules in the structure was randomly picked up and the water clusters surrounding the selected water molecule within 5.0 Å were constructed. Unsaturated chemical bonds were terminated by hydrogen atoms. The calculated spectra of more than 20 clusters were accumulated to give the theoretical XES spectra at each temperature.

The experimental XES results of the dehydration process of **1•$H_2O$** revealed spectroscopic information of the flexible water molecules located at the central regions of the pores, because the water molecules located at the pore surface might be trapped more strongly than those at pore centers. The experimental XES spectrum showed that the intensity of the $1b_1$'' peak at 526.7 eV exceeded that of $1b_1$' at 525.8 eV, suggesting that water molecules in the central regions of the pore channel form fewer than four hydrogen bonds in a distorted pattern.[3] Considering a time scale of the XES measurement and the measurement conditions, the experimental spectra contained averaged spectroscopic information of flexible water molecules located at the central regions of the pores and the vacant form. Thus, for the reproduction of the experimental XES results, simulated XES spectra for the dehydration process of **1•$H_2O$** were obtained by a linear combination of the spectra. As a result, the simulated XES spectra successfully reproduced the experimental features and supported the interpretation based on the experimental observations.

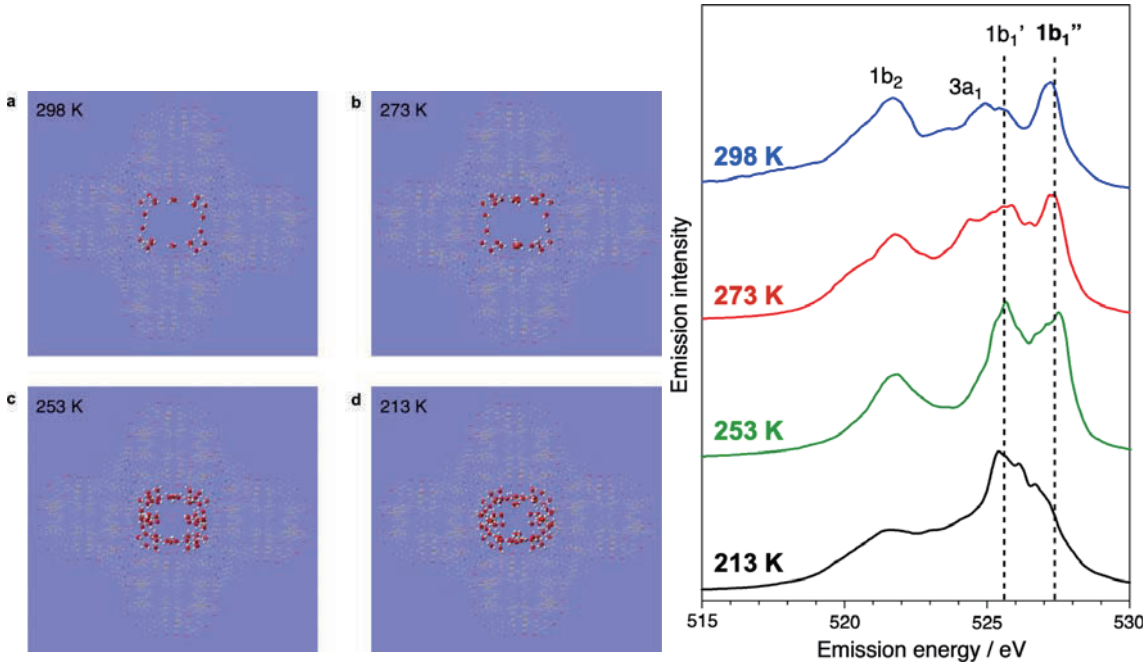


**FIGURE 1.** (left) The molecular structures of **1•$H_2O$** for the calculation at 213, 253, 273 and 253 K, whose structure were based on the X-ray structures. (right) The simulated XES spectra of the water clusters formed at the pore surface.

## REFERENCES


1. O. Björneholm, M. H. Hansen, A. Hodgson, L.-M. Liu, D. T. Limmer, A. Michaelides, P. Pedevilla, J. Rossmeisl, H. Shen, G. Tocci, E. Tyrode, M.-M. Walz, J. Werner, and H. Bluhm, *Chem. Rev.*, **116**, 7698-7726 (2016).
2. E. Brini, C. J. Fennell, M. Fernandez-Serra, B. Hribar-Lee, M. Lukšič, and K. A. Dill, Chem. Rev. **117**, 12385-12414 (2017).
3. S. Horiuchi, S. Ogura, Y. Ikemoto, H. Kiuchi, K. Tatsuta, Y. Tomiyori, Y. Harada, *Activity Report of Synchrotron Radiation Laboratory*, ISSP, The University of Tokyo, 2022.
4. M. P. Ljungberg, I. Zhovtobriukh, O. Takahashi, and L. G. M. Pettersson, *J. Chem. Phys.* **146**, 134506 (10 pages) (2017).
5. O. Takahashi, R. Yamamura, T. Tokushima, and Y. Harada, *Phys. Rev. Lett.* **128**, 086002 (5 pages) (2022).
6. L. G. M. Pettersson and O. Takahashi, *Theor. Chem. Acc.* **140**, 162 (13 pages) (2021).
7. M. J. Frisch et al., *Gaussian 09*, Revision B.01 (Gaussian, Inc., Wallingford, CT, 2010).
8. L. W. Chung, W. M. C. Sameera, R. Ramozzi, A. J. Page, M. Hatanaka, G. P. Petrova, T. V. Harris, X. Li, Z. Ke, F. Liu, H.-B. Li, L. Ding, and K. Morokuma, *Chem. Rev.* **115**, 5678–5796 (2015).

24BU019

# Ionization threshold in MALDI-MS based on the strength of matrix hydrogen bonds

Shunshuke Izumi[a], Kodai Matsuo[b] and Osamu Takahashi[c]

[a] *Graduate School of Integrated Sciences for Life, Hiroshima University, Higashi-hiroshima, Hiroshima 739-0046, Japan*
[b] *Department of Chemistry, Faculty of Science, Hiroshima University, Higashi-hiroshima, Hiroshima 739-0046, Japan*
[c] *Research Institute for Synchrotron Radiation Science, Hiroshima University, Higashi-hiroshima, Hiroshima 739-0046, Japan*

**Keywords:** MALDI-MS, IR

In mass spectrometry (MS), matrix-assisted laser desorption/ionization (MALDI) is an ionization technique that uses a laser energy-absorbing matrix to create ions from large molecules with minimal fragmentation [1]. It has been applied to the analysis of biomolecules (biopolymers such as DNA, proteins, peptides, and carbohydrates) and various organic molecules (such as polymers, dendrimers, and other macromolecules), which tend to be fragile and fragmented when ionized using more conventional ionization methods. It is known that the phenolic hydroxyl group is an important proton source for ionization of sample molecules [2]. However, differences in the ionization efficiency were observed among the matrices with phenolic hydroxyl groups. In the present study, we discuss the hydrogen bonds of the hydroxyl groups in the matrix and the relationship between the strength of the hydrogen bonds in the matrix and ionization threshold.

There are various matrices with low ionization thresholds, such as α-cyano-4-hydroxyciannamic acid (CHCA) and matrices with high ionization thresholds, such as dihydroxybenzoic acid (DHBA). Matrices with high ionization thresholds showed broad OH stretching vibrations at 3000 $cm^{-1}$ in the IR spectrum. This broad OH stretching vibration indicated the presence of strong hydrogen bonds. This relationship between the ionization threshold and IR spectrum can also be observed between caffeic acid and dihydrocaffeic acid. In the present study, dihydrocaffeic acid was exposed to UV light, which generated sufficient energy to break the hydrogen bond, and *in situ* IR measurements were performed.

Attenuated total reflection Fourier-transform infrared spectrometry (ATR FT-IR) spectra were measured using a FT-IR spectrophotometer (Frontier FT-IR, Perkin-Elmer, MA) equipped with an ATR diamond cell (Universal ATR Sample Accessory) at room temperature. The spectral resolution was 4 $cm^{-1}$ and the cumulative number was 10. As UV light source, LED light source (CL-1501, Asahi Spectra) with 355 nm head unit was used.

The results are shown in Fig. 1 and 2. The peak of the IR spectrum assigned to OH stretching became sharp owing to the breaking of hydrogen bonds.

The present results suggest that irradiation with light cause hydrogen bonds between the matrix molecules to be lost, and the energy required to extract protons from the matrix decreases. Thus, it is concluded that if the hydrogen bonds in the matrix are strong, energy is required to break them, so the ionization threshold becomes large and the ionization efficiency decreases.

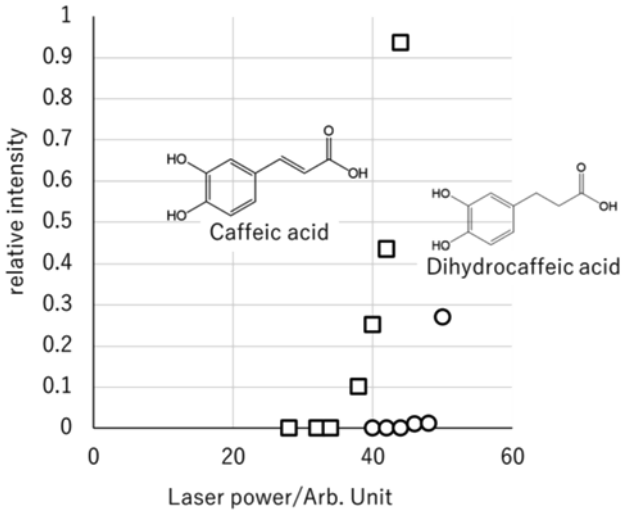


**FIGURE 1**. Ionization threshold for angiotensin II when caffeic acid (square) and dyhydrocaffeic acid (circle) are used as matrices.

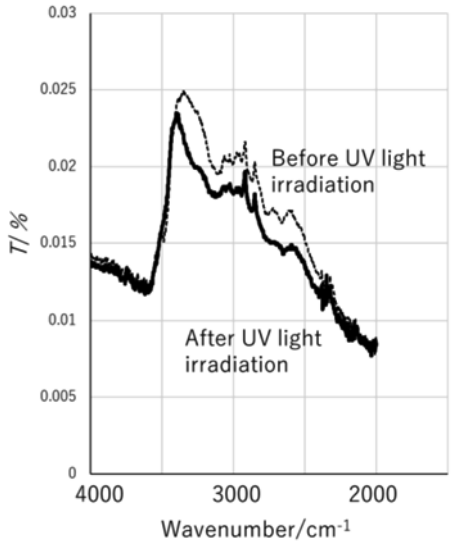


**FIGURE 2.** Change in IR spectrum when dihydrocaffeic acid is irradiated with UV light. Before UV light irradiation (dotted line). After UV light irradiation (thick line).

## REFERENCES

1. F. Hillenkamp, M. Karas, R. C. Beavis, T. Brian, *Anal. Chem.*, **63**, 1193A-1203A (1991).
2. G. R. Kinsel, R. Knochenmuss, P. Setz, C. M. Land, S.-K. Goh, E. F. Archibong, J. H. Hardesty, and D. S. Marynick, *J. Mass Spectrom.*, **37**, 1131-1140 (2002).

24BU020

# Theoretical study of functional liquid membrane

Osamu Takahashi[a], Hitoshi Washizu[b], Yoshiki Ishii[c], and Yoshihisa Harada[d]

[a] *Research Institute for Synchrotron Radiation Science, Hiroshima University, Higashi-hiroshima, Hiroshima 739-0046, Japan*
[b] *Graduate School of Information Science, University of Hyogo, Chuo-ku, Kobe, Hyogo 650-0047, Japan*
[c] *School of Frontier Engineering, Kitazato University, Sagamihara, Kanagawa 252-0373, Japan*
[d] *Institute of Solid State Physics, The University of Tokyo, Kashiwa, Chiba 277-8581, Japan*

**Keywords:** Liquid crystal membrane, molecular dynamics simulation, density functional theory, x-ray emission spectroscopy

Membrane technology to produce fresh water from seawater and contaminated water is extremely attractive because it is low energy and simple to implement [1,2]. Recently, self-assembled liquid crystalline membrane materials with uniform pore size in the nano or sub-nano class have been developed. By controlling the hydrophilic groups in the films, liquid crystalline films with different separation capacities can be produced. In order to develop membranes with more effective separation ability, it is important to understand the nature of water in the pores, i.e., the structure of hydrogen-bonded water in the nanochannel.

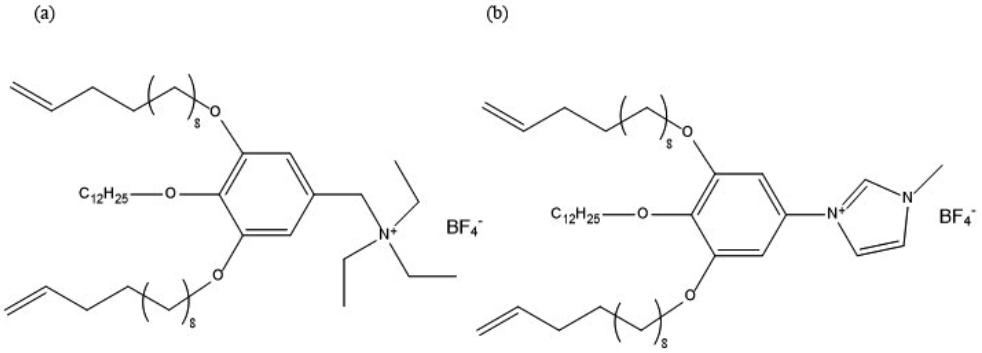


**FIGURE 1.** Molecular structure of ILC. (a) benzyltriethyl- ammonium and (b) benzylimidazorium system.

Soft X-ray emission spectroscopy (XES) measurements were performed to investigate the structure of water in the pores of liquid crystal films. In the case of liquid crystal membranes (ILCs) with benzyltriethylammonium groups, observed spectra of the water in the membranes resembles that in $MgSO_4$ solution when compared to that in NaCl solution, suggesting that this explains the water permeability [2]. In the present study, we constructed membrane models of two types of liquid crystal membranes with triethylammonium and imidazolium groups (Fig. 1) as typical examples of membranes by molecular dynamics (MD) simulations [3]. In addition, X-ray emission spectroscopy (XES) calculations were performed to explore the structure of water in the pores.

MD simulations were performed to simulate the behavior of ILCs at the room temperature using GROMACS [4]. The OPLS-AA force field for ILCs and TIP4P/2005 models for water molecules was used in the whole simulations.

In the theoretical investigation for the XES spectra, electronic structure calculations were obtained within the framework of the density functional theory using the code deMon2k [5]. The basis sets and functionals were used as same as those reported previously [6,7]. The semiclassical Kramers-Heisenberg (SCKH) formula was applied to mimic the experimental XES spectra [6]. To correct entanglement of the potential energy curve and discontinuous of the transition moment, a new scheme with the genetic algorithm was applied [8]. Although the intensities of $1b_2$ and $3a_1$ peaks are overestimated in the calculations, the contributions for $1b_2$ and $3a_1$ peaks were not discussed.

We focus on the double peaks seen around 528 and 529 eV, which are attributed to the $1b_1$ state of water. Results are shown in Fig. 2. In our previous study [7], these peaks originate from two different structures that induce different dynamics. The peak structures differ depending on the type of solution and the membrane structure. In water in the membrane, the relative intensity of the double peaks is independent of the water concentration (experimentally corresponding to the water pressure in the membrane). In the case of the triethylammonium system, the intensity between the double peaks tends to be higher at 3M. This reflects the difference in dynamics resulting from the various hydrogen bonding modes. In the case of the imidazolium system, the spectrum is independent of the water concentration. These differences may reflect differences in the hydrophilicity of the functional groups. The water in the membrane is more similar to that in the $MgSO_4$ solution, providing a qualitative explanation for the permeability of the membrane.

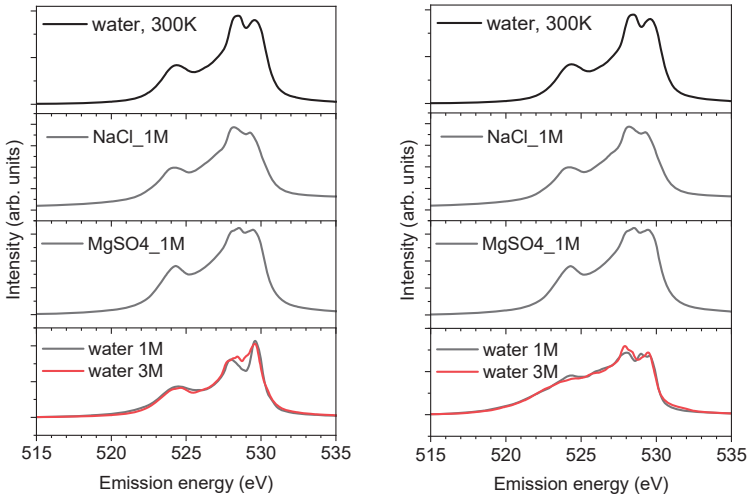


**FIGURE 2.** XES spectra of liquid water, 1M NaCl, 1M $MgSO_4$, and water in ILCs. Left and right panels means triethylamine and imidazorium ILCs, respectively.

## REFERENCES


1. M. Henmi, K. Nakatsuji, T. Ichikawa, H. Tomioka, T. Sakamoto, M. Yoshio, and T. Kato, *Adv. Mater.*, **24**, 2238-2241 (2012).
2. R. Watanabe, T. Sakamoto, K. Yamazoe, J. Miyawaki, T. Kato, and Y. Harada, *Ang. Chem. Int. Ed.*, **59**, 23461-23465 (2020).
3. Y. Ishii, N. Matubayasi, G. Watanabe, T. Kato, and H. Washizu, *Sci. Adv.*, **7**, eabf0669 (14 pages) (2021).
4. M. J. Abraham, T. Murtola, R. Schulz, S. Páll, J. C. Smith, B. Hess, and E. Lindahl, *SoftwareX*, **1-2**, 19-25 (2015).
5. A. M. Köster et al., Demon2k ver.5 (2018).
6. M. P. Ljungberg, A. Nilsson, and L. G. M. Pettersson, *Phys. Rev. B*, **82**, 245115 (11 pages) (2010).
7. O. Takahashi, R. Yamamura, T. Tokushima, and Y. Harada, *Phys. Rev. Lett.,* **128**, 086002 (5 pages) (2022).
8. L. G. M. Pettersson and O. Takahashi, *Theor. Chem. Acc.,* **140**, 162 (13 pages) (2021).

24BU021

# Theoretical XES calculations of aqueous hydrogen peroxide

Osamu Takahashi[a], Zhong Yin[b], Yoshihisa Harada[c], Stephan Thuermer[d], Johan Gråsjö[e] and Jan-Erik Rubensson[f]

[a] *Research Institute for Synchrotron Radiation Science, Hiroshima University, Higashi-hiroshima, Hiroshima 739-0046, Japan*
[b] *International Center for Synchrotron Radiation Innovation Smart, Tohoku University, Sendai 980-8577, Japan*
[c] *Institute of Solid State Physics, The University of Tokyo, Kashiwa, Chiba 277-8581, Japan*
[d] *Department of Chemistry, Kyoto University, Kyoto 606-8502, Japan*
[e] *Department of Medicinal Chemistry, Uppsala University, Box 516, 751 20 Uppsala, Sweden*
[f] *Department of Physics and Astronomy, Uppsala University, Box 516, 751 20 Uppsala, Sweden*

**Keywords:** Hydrogen peroxide, Resonant inelactic X-ray scattering, Density functional theory.

The importance of hydrogen peroxide ($H_2O_2$) can be exemplified by its occurrence as a constituent in different biological processes [1], industrial processes [2], and atmospheric chemistry [3,4], where its interaction with electromagnetic radiation is important in reactions and reaction chains. Because of its large similarity to water, for example by being a small polar, hydrogen bonding molecule consisting of just oxygen and hydrogen, studies of $H_2O_2$ could also give valuable results for the understanding of water by comparing similarities and differences to water [5].

In resonant inelastic X-ray scattering (RIXS) processes, the initial and final states are, under certain circumstances, identical to the initial and final states of the UV absorption processes. The results of RIXS measurements could therefore, under correct circumstances, be directly compared to experimental and theoretical studies of UV absorption. An advantage of RIXS is that it offers the opportunity to excite selected levels of unoccupied states, and comparing the RIXS spectra to UV absorption could aid in assigning the excitations. Furthermore, using off-resonance excitations (de-tuning), the lifetime of the intermediate state could be controlled to some extent. When dissociation occurs, the dynamics of the dissociation could be estimated and spectral information of the dissociation products could be obtained.

In this report, RIXS spectral calculations of an aqueous solution of $H_2O_2$ for resonant and non-resonant excitations are presented. These spectra are compared with the measured spectra of $H_2O_2$.

To construct the model structures in aqueous $H_2O_2$, molecular dynamics (MD) simulations were performed at room temperature using GROMACS [6]. The OPLS-AA force fields for the $H_2O_2$ and TIP4P/2005 models for water molecules were used in all simulations. Using a fixed number of particles, pressure, and temperature (NPT) ensemble at 300 K and 1 bar, simulations were propagated with a time step of 0.1 fs. From several snapshots of the simulations, cluster models including 20 molecules centered a core-excited $H_2O_2$ molecule were produced. The size of this cluster model corresponds to the size of the second shell region obtained from the radial distribution function. In the theoretical investigation of RIXS spectra, electronic structure calculations were performed within the framework of density functional theory (DFT) using the code deMon2k [7]. The basis sets and functionals were the same as those previously reported [8,9]. For the sampled clusters, core-hole excited-state dynamics simulations were propagated for 20 fs with a time step of 0.25 fs. These lengths of time were sufficient to produce the spectral resolution required for a comparison of these results with those of the experimentally determined decay processes. The relative peak intensities of the spectra from the core-hole excited-state dynamics simulations were calculated for each geometry using MD simulations. The semiclassical Kramers-Heisenberg (SCKH) formula was applied to mimic experimental XES spectra [8]. To correct the entanglement of the potential energy curve and the discontinuity of the transition moment, a new scheme with a genetic algorithm was applied [10]. Although the intensities of $1b_2$ and $3a_1$ peaks are overestimated in the calculations, the contributions for $1b_2$ and $3a_1$

peaks were not discussed.

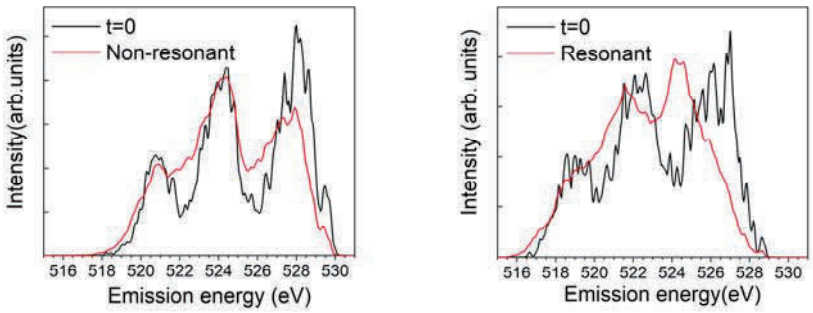


**FIGURE 1.** RIXS spectra of $H_2O_2$ for (left) non-resonant and (right) resonant excitations. Spectra for t=0 are also shown in both cases.

The calculated results are shown in Fig. 1. In both cases, three large peaks can be seen. This corresponds to the experimental results, which are not shown in this report. In particular, we focus on the highest peak. For the non-resonant excitation, three large peaks will be seen. On the other hand, for the resonant excitation, the highest peak at 524.2 eV is shifted to lower than that for non-resonant one. This is caused by fast core-hole excited-state dynamics. In Fig. 2, O-O bond propagations as a function of time following core excitation for non-resonant and resonant excitations are shown. In both cases, bond dissociation for an O-O bond can be seen, and the dynamics for the resonant excitation are much faster than those for the non-resonant excitation. To understand this more explicitly, the potential energy curve (PES) of $H_2O_2$ along the O-O distance is depicted. It is noted that the equilibrium bond distance of the O-O bond is approximately 1.4 Å. The slope of the PES for the resonant excitation is more negative than that for non-resonant excitation.

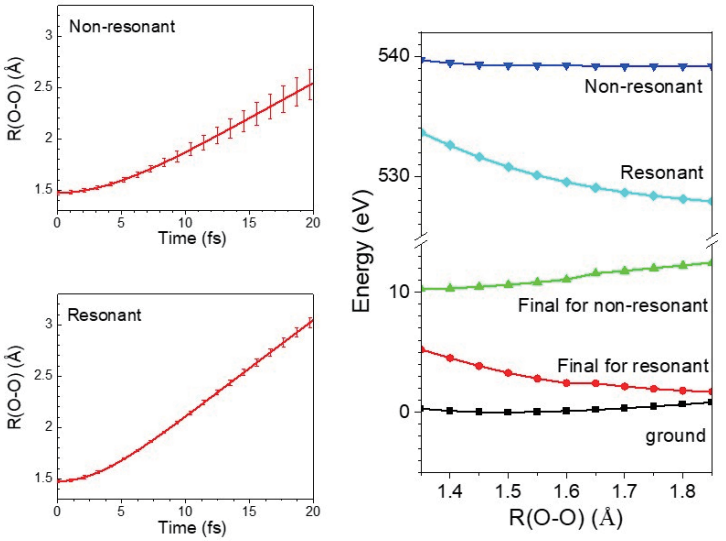


**FIGURE 2.** (left) O-H bond propagations as a function of time for non-resonant and resonant excitations. (right) potential energy curves of $H_2O_2$ single molecule along to O-O distance.

## REFERENCES


1. J. A. Imlay, *Ann. Rev. Microbio.*, **57**, pp. 395-418 (2003).
2. F. J. Beltrán, J. Encinar, and J. F. González, *Water Res.*, **31**, 2415-2428 (1997).
3. Y. Zuo and J. Hoigne, *Environmental Science & Technology*, **26**, 1014-1022 (1992).
4. H. Sakugawa, I. R. Kaplan, W. Tsai, and Y. Cohen, *Environmental Science & Technology,* **24**, 1452-1463 (1990).
5. P. A. Giguère, *J. Raman Spectrosc.*, **15**, 354-359 (1984).
6. M. J. Abraham, T. Murtola, R. Schulz, S. Páll, J. C. Smith, B. Hess, and E. Lindahl, SoftwareX **1-2**, 19-25 (2015).
7. A. M. Köster et al., Demon2k ver.5 (2018).
8. M. P. Ljungberg, A. Nilsson, and L. G. M. Pettersson, Phys. Rev. B **82** (24), 245115 (11 pages) (2010).
9. O. Takahashi, R. Yamamura, T. Tokushima, and Y. Harada, *Phys. Rev. Lett.* **128**, 086002 (5 pages) (2022).
10. L. G. M. Pettersson and O. Takahashi, *Theor. Chem. Acc.* **140**, 162 (13 pages) (2021).